

Isogeometric analysis of C^1/G^1 dual mortaring and its application for multi-patch Kirchhoff-Love shell

Di Miao

Advisor: Michael J. Borden

*Department of Civil and Environmental Engineering
Brigham Young University
368 CB, Provo, UT 84602, USA*

1. Introduction

Isogeometric analysis was introduced by Hughes et. al. [49] in 2005, as a novel discretization technology. Since then, it attracted considerable attentions from the academic world and is enjoying explosive growth. The idea behind isogeometric analysis is to use the same basis functions for the geometric modeling and computational analysis. While the main aim of isogeometric analysis is to eliminate the geometric approximation error, it has been observed that, compared to traditional C^0 finite element, higher regularity Non-uniform Rational B-splines (NURBS) provide higher efficiency per degree of freedom [5, 29, 30]. Meanwhile, high regularity basis functions allow us to solve higher order partial differential equations (PDEs), e.g. the biharmonic equation [66, 56, 53], the Kirchhoff-Love shell problem [58, 57, 59] and the Cahn-Hilliard equation [42, 17, 16].

However, the higher dimensional NURBS basis functions are obtained by a tensor product of one-dimensional NURBS basis functions, which imposes limitations on its feasibility for analysis. Considering a scenario that a refinement is applied to a region of interest, however, for the tensor-product domain, it also introduces control points far from that region, which dramatically increases the problem size.

The adaptive finite element technique try to automatically refine a mesh in an optimal fashion so that a desirable discretization error level is achieved

22 with the fewest degrees of freedom. Based on the solution from a coarse
23 mesh, a *posteriori* error estimator provides a guidance for deciding where
24 and how to refine a mesh. It can increase the convergence rate, particularly
25 when singularities are present. However, this promising technique can not
26 be applied directly to NURBS mesh, as it does not support local refinement.

27 Since high smoothness basis function can be used in Isogeometric analy-
28 sis, the numerical approximation of high order PDEs can be realized in the
29 framework of the standard Galerkin formulation. However, without intro-
30 ducing mesh degenerations, it is impossible to parameterize geometries with
31 sharp corner or kink by high continuity meshes.

32 2. Literature review

33 To circumvent the shortcomings discussed above, various methods have
34 been proposed. The purpose of this section is to provide an overview of the
35 popular methods that endow B-spline meshes with multi-patch coupling and
36 local refinement abilities.

37 2.1. Local refinable splines

38 In 1988, Forsey and Bartels [40] introduced the hierarchical B-spline re-
39 finement algorithm, which can restrict the influence of refinement to the lo-
40 cality. The algorithm is achieved by a re-representation process that replaces
41 each basis function by an equivalent linear combination of a set of basis func-
42 tions defined by nested knot vectors. However, due to the lack of a natural
43 control grid, the hierarchical B-spline has not been widely recognized in the
44 CAD society, and a few applications can be found in geometric design. Re-
45 cently, this technique has been extended to Isogeometric Analysis, by Vuong
46 *et al.* [87]. Owing to the construction strategy, the resulted hierarchical
47 basis function are linearly independent and retain the maximal regularity,
48 which renders the hierarchical B-spline a good candidate for analysis. The
49 numerical tests demonstrate that the use of the hierarchical B-spline lead to
50 a superior performance for problems with corner singularity. A subdivision-
51 based hierarchical B-spline was proposed by Bornemann *et al.* [18], to tackle
52 the intricate algorithms in the software implementation of hierarchical B-
53 splines. The subdivision scheme establishes algebraic relations between the
54 basis functions and their coefficients defined on different refinement level
55 of the mesh and greatly ease the implementation of hierarchical B-splines.
56 Consecutively, the truncated basis for hierarchical splines (THB-spline) was

57 introduced by Giannelli *et al.* [41]. THB-splines is created by eliminating
58 from the coarse hierarchical basis function the contribution corresponding to
59 the subset of finer basis functions. Besides all the nice properties of hierarchi-
60 cal B-splines, the THB-splines obtain smaller support and form a partition
61 of unity, which lead to sparser matrices and lower condition numbers.

62 However, all the above hierarchical B-splines are still under the tensor
63 product formulism, which restricts hierarchical B-splines to a global rectan-
64 gular parametric domain. In order to represent complex topologies, subdivi-
65 sion schemes are widespread in geometry processing and computer graphics.
66 Among the most popular subdivision schemes are the Catmull-Clark [23],
67 Doo-Sabin [31] and Loop's [64] scheme. For Isogeometric Analysis, Wei *et*
68 *al.* [88] introduced truncated hierarchical Catmull-Clark subdivision (THCCS)
69 that can handle extraordinary nodes involved in complex topologies. THCCS
70 inherits the surface continuity of Catmull-Clark subdivision, namely C^1
71 continuity at extraordinary points and C^2 continuity elsewhere. Loop subdivi-
72 sion surfaces provides similar regularity properties as THCCS and has been
73 applied to Isogeometric Analysis in [52, 71] to generate triangular meshes.
74 One of the limitations in the implementation of subdivision meshes is that
75 the basis function around the extraordinary point is composed of piecewise
76 polynomial functions with an infinite number of segments, which leads to
77 insufficient integration by Gauss quadrature rule. To deal with this issue,
78 various quadrature rules and adaptive strategies have been examined in [67]
79 for Poisson problem on the disk and in [51] for fourth order PDEs.

80 In 2003, Sederberg *et al.* [79] introduced T-splines, which allows the
81 existence of T-junctions in the control grid, so that lines of control points
82 need not traverse the entire control grid. Thus, local refinement can be
83 realized by introducing T-junctions around interested region. Since the con-
84 cept of T-splines is a generalization of NURBS technology, it can be used
85 to merge NURBS surfaces that have different knot-vectors at the intersec-
86 tion. Therefore, the T-splines are also suitable to address trimmed multi-
87 patch geometries. Due to the desirable features of T-splines, Bazilevs *et al.*
88 [4] explored this technology in Isogeometric Analysis, and numerical results
89 demonstrated its potential for solving structural and fluid problems. By
90 utilizing the Bézier extraction operator, a finite element data structure for
91 T-splines [78] was developed to ease the incorporation of T-splines into ex-
92 isting finite element codes. However, it has been proven [22] that the original
93 definition of T-splines is not sufficient to ensure the linear independence of
94 the basis functions. To circumvent this issue, analysis suitable T-splines [63]

95 was developed by applying an additional constraint that no two orthogonal
96 T-junction extensions are allowed to intersect. Subsequently, the mathematical
97 properties of analysis suitable T-splines were studied in [62, 91], and it
98 has been successfully applied to the boundary element method [77]. Mean-
99 while, an adaptive local h-refinement algorithm with T-splines and a local
100 refinement of analysis-suitable T-splines were introduced by Döfel *et al.* [37]
101 and Scott *et al.* [76], respectively. However, for both algorithm, the refined
102 mesh is not as local as one could hope and this problem might be severe in
103 3D.

104 *2.2. Multi-patch geometrically continuous functions*

105 One of the advantages of Isogeometric Analysis is that it provides basis
106 functions with high smoothness, *i.e.* for p -th order splines, they enjoy up
107 to C^{p-1} continuity within a single patch. Thus, it is possible to directly
108 discretize differential operators of order higher than 2. However, continuity
109 higher than C^0 for multi-patch discretization imposes significant difficulties.
110 The conception of geometric continuity is very important in CAD field [73] for
111 designing smooth multi-patch domain containing extraordinary vertices [72].
112 In the parametric space, the geometric continuity of order s (G^s continuity)
113 is a weaker continuity constraint as compared to C^s continuity, while it has
114 been proved by Giroisser and Peters [43] that G^s continuity in the parametric
115 space is equivalent to C^s continuity of the basis function after the parametric
116 mapping. Thus, the construction of C^s isogeometric functions over a C^0
117 parameterization can be interpreted as geometric continuity G^s of the graph
118 parameterization. Bercovier *et al.* [12] has shown that for multi Bézier
119 patches over an unstructured quadrilateral mesh, as long as the order of
120 polynomial is high enough, there always exists the minimal determining set
121 for a C^1 continuity construction. Moreover, the resulting basis functions do
122 not contain subdivisions around extraordinary vertices.

123 The case of G^1 continuous functions on bilinearly parametrized two-patch
124 B-spline domains was considered by Kapl *et al.* [56], where the C^1 basis
125 functions are constructed and analyzed by numerical tests. It is shown that
126 the space dimensionality heavily depends on the parameterization of two
127 bilinear patch, and optimal convergence is observed on biharmonic problem.
128 However, over-constrained C^1 isogeometric spaces that causes sub-optimal
129 convergence is also observed for certain configurations (*e.g.* two-patch non-
130 bilinear parameterizations and C^{p-1} continuity within the patches for p -th
131 order spline space). A theoretical analysis of the causing of C^1 locking is

132 provided in [25], where the analysis-suitable G^1 geometry parameterization,
133 that allows for optimal approximation of C^1 isogeometric spaces, is identified
134 and testified by numerical examples. The methods in [56] has been extended
135 to bilinearly parameterized multi-patch domains in [53], where the simple
136 explicit formulas for spline coefficients of C^1 basis function is derived and
137 nested C^1 isogeometric spaces are generated. Recently, Kapl *et al.* [55,
138 54] explored the construction of C^2 isogeometric functions on multi-patch
139 geometries and utilized the C^2 isogeometric spaces for 6-th order PDE.

140 Although the geometrically continuous functions circumvent the use of
141 subdivisions for domains with extraordinary vertices, the requirement of C^0
142 parameterization averts local mesh refinement, and lower continuity is re-
143 quired to avoid C^1 locking effect. Thus, its implementation can be complex
144 and it may not be a potential candidate for analysis in more general situa-
145 tions.

146 *2.3. Variational approach for domain coupling*

147 Unlike geometric design, where high continuity basis functions along the
148 intersections of neighboring patches are required for the construction of high
149 quality surface; in analysis, these strong point-wise constraints are unnec-
150 essarily rigorous, a good approximation of PDEs can be made even if these
151 constraints are applied in the weak sense. Moreover, the non-conforming
152 multi-patch coupling is allowed, which maintains the flexibility for the choice
153 of meshes when multi-patch discretization is needed. Mathematically, the er-
154 ror estimation of the non-conforming finite element approximation is based on
155 Strang's lemma [20, 83], which says that for the non-conforming discretized
156 PDEs, the distance between exact solution to the discrete one is bounded by
157 the sum of the approximation error and the consistency error. The approx-
158 imation error measures the failure of discretized finite dimensional space to
159 capture the exact solution, while the consistency error measures the incon-
160 sistency between the exact equation and the discretized equation. Various
161 methods have been developed to eliminate the consistency error and recover
162 optimal convergence, among them are the mortar method (Lagrange multi-
163 plier method), stabilized Lagrange multiplier method, the Nitsche's method
164 and the discontinuous Galerkin (dG) method.

To clearly demonstrate these methods, we consider the following Poisson

problem with homogenous Dirichlet boundary conditions

$$\begin{aligned} -\Delta u &= f, && \text{in } \Omega \\ u &= 0, && \text{on } \partial\Omega \end{aligned} \quad (1)$$

where Ω denote a bounded open domain in \mathbb{R}^d , $d = 2$ or 3 being the dimension of the problem and its boundary is denoted by $\partial\Omega$, in order to simplify the presentation we restrict ourselves to the case of two-dimensional computational domain. The weak form of Equation (1) reads as follow: Find $u \in H_0^1(\Omega)$ such that

$$a(u, v) = l(v), \quad \forall v \in H_0^1(\Omega), \quad (2)$$

where

$$\begin{aligned} a(u, v) &= \int_{\Omega} \nabla u \cdot \nabla v d\Omega, \\ l(v) &= \int_{\Omega} fv d\Omega. \end{aligned} \quad (3)$$

Using the fact that $C^0(\Omega) \subset H^1(\Omega)$, the weak solution can be approximated by considering a finite dimensional continuous function space. Now, we assume that the domain Ω is subdivided into K non-overlapping subdomains or patches Ω_k for $1 \leq k \leq K$, i.e.

$$\bar{\Omega} = \bigcup_{k=1}^K \bar{\Omega}_k \quad \text{and} \quad \Omega_k \bigcap \Omega_l = \emptyset \quad \forall k \neq l. \quad (4)$$

For simplicity, we only consider the case that the intersection of two patches is either empty or vertex or the entire edge, which rules out the possibility of hanging nodes. We denote the common interface of two neighboring subdomains $\Gamma_{kl} = \partial\Omega_k \cap \partial\Omega_l$ so that $\Gamma_{kl} = \emptyset$ if Ω_k is not a neighbor of Ω_l and define the skeleton $\mathbf{S} = \bigcup_{k,l \in K, k \neq l} \Gamma_{kl}$ as the union of all interfaces. A representative example of geometry is presented in Figure 1. We can associate each subdomain a bijective geometric mapping as

$$\mathbf{F}_k(\xi_k, \eta_k) : \hat{\Omega}_k \mapsto \Omega_k \in \mathbb{R}^d, \quad (5)$$

where $\hat{\Omega}_k$ is the parametric domain of k^{th} patch associated with coordinates (ξ_k, η_k) . For the simplicity and without loss of generality, we assume

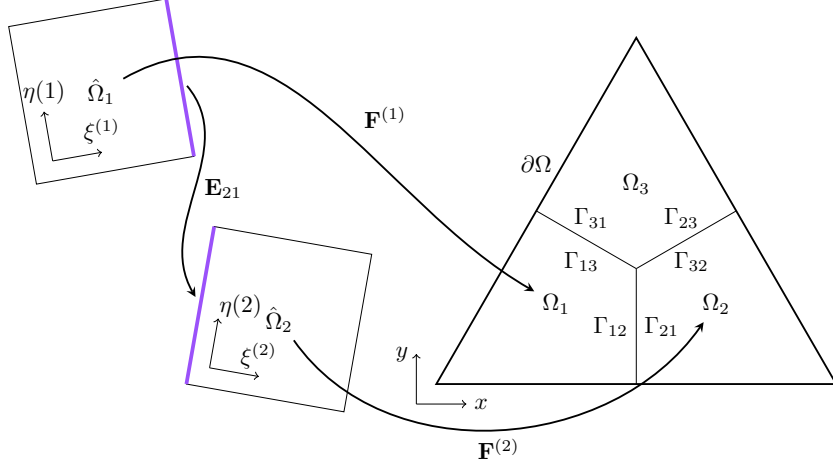


Figure 1: An example of domain decomposition, patches are defined on different parametric domains and are connected via geometric mapping.

¹⁸³ $\hat{\Omega}_k = [0, 1] \times [0, 1]$ for all patches. Due to the difference in the patch pa-
¹⁸⁴ rameterizations, a physical point on the interface can be mapped to different
¹⁸⁵ parametric domains with different coordinates. Owing to non-singular pa-
¹⁸⁶ rameterization, we can establish a bijective transformation from the shared
¹⁸⁷ edge of $\hat{\Omega}_k$ to that of $\hat{\Omega}_l$ by

$$\mathbf{E}_{kl} = (\mathbf{F}_l)^{-1} \circ \mathbf{F}_k. \quad (6)$$

¹⁸⁸

¹⁸⁹ For each Ω_k , we introduce the function space

$$H_*^1(\Omega_k) := \left\{ u \in H^1(\Omega_k) : u = 0 \quad \text{on } \partial\Omega \cap \partial\Omega_k \right\}, \quad (7)$$

¹⁹⁰ now we can define the broken Sobolev space

$$\mathcal{X} := \left\{ u \in L^2(\Omega) : u|_{\Omega_k} \in H_*^1(\Omega_k) \right\}. \quad (8)$$

¹⁹¹ Now, the question is how to approximate the weak solution of Equa-
¹⁹² tion (2) from a finite dimensional subspace of \mathcal{X} . Since functions in \mathcal{X} can be
¹⁹³ discontinuous on the skeleton \mathbf{S} , $a(u, u)$ is no longer coercive (or V-elliptic)
¹⁹⁴ on \mathcal{X} . As a result, directly using a finite dimensional subspace of \mathcal{X} to
¹⁹⁵ discretize Equation (2) will lead to a non-invertible stiffness matrix. Mod-
¹⁹⁶ ications to the weak form is needed, and we will review some of the most
¹⁹⁷ popular methods in this section.

198 2.3.1. Lagrange multiplier method

199 The Lagrange multiplier method (or sometimes called mortar method)
 200 is a domain decomposition technique that allows the coupling of different
 201 discretization schemes or of non-matching triangulation along interior inter-
 202 faces. The inter-element continuity condition is enforced weakly by Lagrange
 203 multipliers. For the Poisson problem, the C^0 continuity constraint is required
 204 on the intersections, in other words, the jump on the skeleton

$$[u]_{\Gamma_{kl}} := u_k - u_l = 0, \quad \forall \quad \Gamma_{kl} \in \mathbf{S}, \quad (9)$$

205 where $u_k = u|_{\Omega_k}$. In order to apply the constraint to the weak form, we
 206 introduce the potential energy functional:

$$\Pi(v) := \frac{1}{2}a(v, v) - l(v). \quad (10)$$

207 The Equation (2) is equivalent to the minimization problem:

$$\inf_{v \in H_0^1(\Omega)} \Pi(v). \quad (11)$$

208 Then, given a function space \mathcal{M} defined on the skeleton, a Lagrange multi-
 209 plier $\mu \in \mathcal{M}$ is used to add the constraint (9) to the potential energy func-
 210 tional (10), and the resulted the potential energy functional for the Lagrange
 211 multiplier method reads

$$\Pi_{LM}(v, \mu) := \Pi(v) + b(\mu, v), \quad (12)$$

212 where

$$b(\mu, v) = \sum_{\Gamma \in \mathbf{S}} \int_{\Gamma} \mu [u]_{\Gamma} d\Gamma. \quad (13)$$

213 The variational formulation of the Lagrange multiplier problem can be de-
 214 rived from the saddle point problem of the potential energy functional (12)

$$\inf_{v \in X} \sup_{\mu \in \mathcal{M}} \Pi_{LM}(v, \mu), \quad (14)$$

215 as, find $(u, \lambda) \in \mathcal{X} \times \mathcal{M}$ such that

$$\begin{cases} a(u, v) + b(v, \lambda) = l(v) & \forall v \in \mathcal{X}, \\ b(u, \mu) = 0 & \forall \mu \in \mathcal{M}. \end{cases} \quad (15)$$

216 The solution of the variational formulation is the infimum in v and the supre-
 217 mum in μ , in other words, it is still a minimization problem in terms of the
 218 primary variable v and any function that violate the constraint will be elim-
 219 inated by the Lagrange multiplier μ . This is the reason why it is called the
 220 saddle point problem. We also denote that the physical meaning of the La-
 221 grange multiplier μ for (12) is the flux of v over the skeleton. A comprehensive
 222 study of the mixed problem (15) can be found in [15].

223 In the discretized problem, for a given discrete space \mathcal{X}_h , the choice of
 224 the discrete Lagrange multiplier space \mathcal{M}_h plays a fundamental role for the
 225 stability of the saddle point problem and the optimality of the discretization
 226 scheme. To ensure the optimality, the function space for Lagrange multiplier
 227 should be judiciously chosen so that the consistency error should converges
 228 at the same rate as that of the approximation error. The feasibility of the
 229 discrete space pair $\mathcal{X}_h \times \mathcal{M}_h$ can be measured by the inf-sup test. The inf-sup
 230 condition is also refered to as the Ladyzhenskaya-Babuska-Brezzi condition
 231 (or simply LBB). It is a crucial condition to ensure the solvability, stabil-
 232 ity and optimality of a mixed problem. For the problem (15), the inf-sup
 233 condition is [15], for $v \neq 0$ and $\mu \neq 0$

$$\inf_{\mu \in \mathcal{M}} \sup_{v \in \mathcal{X}} \frac{|b(v, \mu)|}{\|v\|_{\mathcal{X}} \|\mu\|_{\mathcal{M}}} \geq \beta > 0. \quad (16)$$

234 Since the approximation error of problem (15) is given as

$$\|u - u^h\|_{\mathcal{X}} + \|\lambda - \lambda^h\|_{\mathcal{M}} \leq C \left(\inf_{u^h \in \mathcal{X}^h} \|u - u^h\|_{\mathcal{X}} + \inf_{\lambda^h \in \mathcal{M}^h} \|\lambda - \lambda^h\|_{\mathcal{M}} \right), \quad (17)$$

235 where C is a constant that depends on variables including β but is inde-
 236 pendent of the mesh size h . Hence, in a discretized problem, the inf-sup
 237 condition requires the variable β to be a constant that is independent of the
 238 mesh size.

239 It is well-known that in order to satisfy the LBB-condition a number of
 240 possible natural choices for the approximation space pair $\mathcal{X}_h \times \mathcal{M}_h$ must be
 241 discarded. In particular, the trace space of slave side, specially convenient
 242 from the computational point of view, often do not satisfy the LBB-condition
 243 and can activate pathologies such as spurious oscillations. To remedy this
 244 problem, the most widely used method in the finite element framework is
 245 reducing the dimension of Lagrange multiplier space by two (for 2nd order
 246 PDEs). Specifically, the degree of Lagrange multiplier basis functions at both

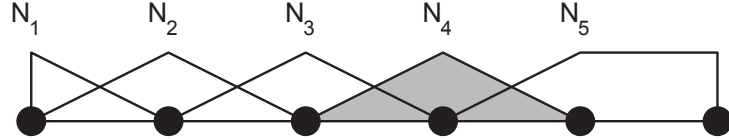


Figure 2: Lagrange multiplier basis functions for the piecewise linear elements, modification on the right end (from Zienkiewicz [92]).

247 ends are reduced by one. This modification has been sucessfully adopted in
 248 [14, 13, 7, 10, 8, 65, 60, 9]. An example of the modified Lagrange multiplier
 249 basis functions are illustrated in Figure 2, where the basis function N_5 is
 250 constant in the right end.

251 In the context of Isogeometric Analysis, the patch coupling problem has
 252 been firstly studied by Hesch and Betsch [47], where the coupling of La-
 253 grangian elements and NURBS elements for 3D nonlinear elastic problem
 254 is validated. To avoid an over constrained linear system, Hesch and Betsch
 255 used a linear Lagrange multiplier space for higher order NURBS coupling. In
 256 [21], the choice of the Lagrange multiplier space has been extensively studied,
 257 it testifies that for equal order pairing, a local degree reduction at extraor-
 258 dinary vertices is required, and another possibility is reducing the degree of
 259 Lagrange multiplier space by two compared to the trace space of slave side.
 260 These choices of Lagrange multiplier spaces are proven to be inf-sup stable
 261 by various numerical examples. In addition to the constraint on the inter-
 262 patch displacement, Bouclier *et al.* [19] considered the constraint on the
 263 traction and claimed that this strategy enables to present a C^1 behavior. In
 264 the numerical test, smoother displacement fields and smoother stress fields
 265 are observed.

266 Another drawback of the implementation of mortar methods is that most
 267 of them introduce Lagrange multipliers as additional variables to enforce
 268 interface constraints weakly, increasing the problem size. Moreover, different
 269 physical fields are involved in the weak form, deteriorating the conditioning
 270 of the global matrix if no appropriate pre-conditioner is applied (detailed
 271 discussion about preconditioning for saddle point problem can be found in
 272 [39, 11, 84]).

273 2.3.2. Dual mortar method

274 To circumvent the increase of problem size, we considering the minimiza-
275 tion problem

$$\inf_{v \in \mathcal{K}} \Pi(v), \quad (18)$$

276 where the function space $\mathcal{K} = \{v \in \mathcal{X} : b(v, \lambda) = 0, \forall \lambda \in \mathcal{M}\}$. The mini-
277 mization problem (18) is indeed equivalent to the saddle point problem (15),
278 the proof can be found in [15]. Note that, since $K \subset X$, the introduce of
279 Lagrange multiplier indeedly reduces the problem size of (18). Meanwhile,
280 the symmetric positive definite structure of the resulting stiffness matrix is
281 preserved. But the construction of the function space K is not a trivial task.

282 To reduce the cost of constructing the function space \mathcal{K} , we use the dual
283 basis functions of the trace space of the slave side as the discrete Lagrange
284 multiplier space. For a given basis function N_i , the dual basis function \hat{N}_j is
285 defined to satisfy

$$\int_{\Gamma} N_i \hat{N}_j d\Gamma = \delta_{ij} \int_{\Gamma} N_i d\Gamma, \quad (19)$$

286 where δ_{ij} is a Kronecker delta function. Of special interest, are biorthogonal
287 basis functions with compact support, especially

$$\text{supp } \hat{N}_i = \text{supp } N_i. \quad (20)$$

288 Due to the biorthogonality, the discrete bilinear form $b(v, \mu)$ forms a diagonal
289 matrix on the slave side, and forms a sparse matrix on the master side.
290 The function space \mathcal{K} can be formulated without additional efforts and all
291 the slave degree of freedom are eliminated in the resulting linear system.
292 Moreover, owing to the local support property the resulting stiffness matrix
293 is a symmetric positive definite sparse matrix. Thus, the dual basis functions
294 are very attractive in the perspective of computational efficiency.

295 Figure 3 shows an example of dual basis functions corresponding to the
296 basis functions in Figure 2. Again, order reduction is made at the right end.
297 The dual mortar method was first introduced in [89] for first order finite
298 element. This method has been extended to higher order degree elements in
299 [61], to three-dimensional problem in [90] and to contact problem [48, 74].

300 In isogeometric analysis framework, a master-slave type mortar method
301 has been suggested by Dornisch *et al.* [34], where the weakly applied con-
302 straint is represented as a master-slave relation and the the slave interface
303 degrees of freedom (DOF) can be condensed out of the global linear system.

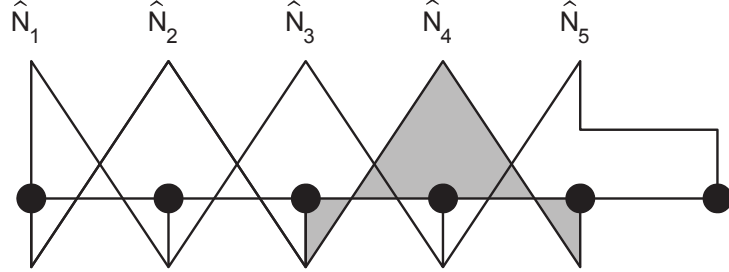


Figure 3: Dual Lagrange multiplier basis functions for the piecewise linear elements, modification on the right end (from Zienkiewicz [92]).

304 Recently, Dornisch *et al.* extended this research to multiple patch coupling in
 305 [36, 33], where different types of dual basis functions are applied as the basis
 306 of Lagrange multipliers. The numerical results demonstrate that the approx-
 307 imate dual basis functions yield accurate result and generate sparse global
 308 matrix due to the local support. The concept of dual mortar methods is also
 309 utilized in [80] for contact problem in Isogeometric analysis framework. Coox
 310 *et al.* [27] proposed an interesting approach to establish the master-slave mor-
 311 tar method and implemented this approach in [26] to form boundary element
 312 analysis on complex manifold. In this approach, the master-slave relation are
 313 formed by knot insertion algorithm and pseudo-inverse.

314 *2.3.3. Perturbed Lagrangian method*

315 Applying constraint by Lagrange multiplier leads to a saddle point prob-
 316 lem, of which the discrete Lagrange multiplier basis functions cannot be
 317 chosen independently of that of primal variable and special treatment is
 318 required on the cross point to ensure the solvability and optimality of the
 319 discretized system. The stiffness matrix for the discrete problem arising from
 320 the Lagrangian multiplier method always contains both positive and negative
 321 eigenvalues, for which iterative methods are known to be less efficient than for
 322 symmetric positive definite systems. To ensure the invertibility of the stiff-
 323 ness matrix, a quadratic penalty term is added to the energy functional (12),
 324 as

$$\Pi_{PLM}(v, \mu) := \Pi_{LM}(v, \mu) - \frac{1}{2\epsilon} \sum_{\Gamma \in S} \int_{\Gamma} \mu^2 d\Gamma, \quad (21)$$

325 where the penalty term is scaled by a parameter ϵ . The resulted func-
 326 tional (21) is referred to as perturbed Lagrangian and the last term is often

327 called stablization term. The resulted variational formulation is stated as

$$\begin{cases} a(u, v) + b(v, \lambda) = l(v) & \forall v \in \mathcal{X}, \\ b(u, \mu) - \frac{1}{\epsilon} \sum_{\Gamma \in \mathbf{S}} \int_{\Gamma} \mu \lambda d\Gamma = 0 & \forall \mu \in \mathcal{M}. \end{cases} \quad (22)$$

328 As $\epsilon \rightarrow \infty$, the solution obtained from (22) will converge to the solution ob-
329 tained by the classical Lagrange multiplier method. For $0 < \epsilon < \infty$, any solu-
330 tion that inconsistent with the constraint will not be fully prohibited, but will
331 be penalized by the stability term. And the rank of discrete stiffness matrix is
332 preserved no matter whether the discrete space pair $\mathcal{X}_h \times \mathcal{M}_h$ fulfills the inf-
333 sup condition or not. However, for a moderate ϵ , the perturbed Lagrangian
334 method is inconsistent with the classical Lagrange multiplier method, and
335 the increase of ϵ will deteriorate the conditioning of stiffness matrix.

336 The perturbed Lagrangian method has been utilized in [81] for contact
337 problem and [35, 1] for domain decomposition problem in isogeometric anal-
338 ysis framework.

339 2.3.4. Stabilized Lagrange multiplier method

340 To fully circumvent the inf-sup condition for imposing Dirichlet boundary
341 by Lagrange multiplier, Barbosa et. al. [3] added a new penalty like term
342 to the energy functional (12) to enhance the stability. Unlike perturbed
343 Lagrangian method where the penalty term is inconsistent with the original
344 problem, the new term proposed by Barbosa maintaining the consistency.
345 The energy functional of stablized Lagrange multiplier method is given as

$$\Pi_{SLM}(v, \mu) := \Pi_{LM}(v, \mu) - \sum_{\Gamma \in \mathbf{S}} \frac{h}{2\gamma} \int_{\Gamma} (\mu + \left\{ \frac{\partial v}{\partial n} \right\})^2 d\Gamma, \quad (23)$$

346 where n is the normal vector of the interface, h is the mesh size on the
347 intersection, γ is a user defined constant, the average operator

$$\{u\}_{\Gamma_{kl}} := \frac{1}{2} u_k + \frac{1}{2} u_l. \quad (24)$$

348 Since the physical meaning of the Lagrange multiplier is the flux on the
349 intersection, the stabilization term in (23) is consistent with the original
350 problem. The resulted variational formulation is stated as

$$\begin{cases} a(u, v) + b(v, \lambda) - \frac{h}{\gamma} \sum_{\Gamma \in \mathbf{S}} \int_{\Gamma} \frac{\partial v}{\partial n} (\lambda + \left\{ \frac{\partial u}{\partial n} \right\}) d\Gamma = l(v) & \forall v \in \mathcal{X}, \\ b(u, \mu) - \frac{h}{\gamma} \sum_{\Gamma \in \mathbf{S}} \int_{\Gamma} \mu (\lambda + \left\{ \frac{\partial u}{\partial n} \right\}) d\Gamma = 0 & \forall \mu \in \mathcal{M}. \end{cases} \quad (25)$$

351 The stabilization parameter γ needs to be carefully chosen. If γ is too large,
 352 the method degrades to a penalty-type method, with sub-optimal accuracy
 353 in the asymptotic limit. If γ is too small, the method becomes unstable.
 354 Recall the trace inequality

$$\|h^{\frac{1}{2}} \frac{\partial u}{\partial n}\|_{\partial\Omega_k}^2 \leq C \|\nabla u\|_{\Omega_k}^2. \quad (26)$$

355 It has been shown [50] that the mixed formulation (25) fulfills the inf-sup
 356 condition if $\gamma > 2C$. The constant C can be approximated by discretize
 357 the norms in the inequality (26) and solve the resulting discrete eigenvalue
 358 problem.

359 It has been demonstrated that there is a close connection with the sta-
 360 bilized Lagrange multiplier method and Nitsche's method in the context of
 361 setting the Dirichlet boundary conditions [82] and in the context of domain
 362 decomposition [46, 45, 50]. Tur et. al. [86] utilized this method to solve
 363 both small and large deformation contact problems and obtained optimal
 364 convergence rate for linear elements. To our knowledge, this method has not
 365 been applied in the isogeometric analysis framework yet.

366 2.3.5. Discontinuous Galerkin method

367 Discontinuous Galerkin method (or Nitsche's method) was introduced in
 368 1971 [69] for handling Dirichlet boundary conditions in the weak sense. Dis-
 369 continuous Galerkin method resembles a mesh-dependent penalty method.
 370 Unlike the standard penalty method, which is not consistent unless the
 371 penalty coefficient goes to infinity, discontinuous Galerkin method is consis-
 372 tent with the original problem. Moreover, no additional unknown (Lagrange
 373 multiplier) is needed and no discrete inf-sup condition must be fulfilled, con-
 374 trarily to mixed methods. Meanwhile, additional term are added into the
 375 weak form to ensure the ellipticity of the problem.

376 To develop the weak form of discontinuous Galerkin method for homoge-
 377 neous Poisson problem, we start by multiplying (1) by a test function $v \in X$
 378 and integrating by parts, we obtain

$$a(u, v) - \sum_{\Gamma \in \mathbf{S}} \int_{\Gamma} \left\{ \frac{\partial u}{\partial n} \right\} [v] d\Gamma = l(v). \quad (27)$$

379 However, if we consider the right-hand side as a bilinear form, it is not
 380 coercive. In other words, this problem is not well-posed, since coercive implies

381 the uniqueness of solution. Meanwhile, this bilinear form is not symmetric.
 382 To recover the symmetry and coercivity of the bilinear form, additional terms
 383 are needed. To maintain the consistency, the added terms must vanish for
 384 the true solution. This lead to the following weak form: find $u \in X$ such
 385 that

$$a(u, v) - \sum_{\Gamma \in \mathbf{S}} \int_{\Gamma} \left\{ \frac{\partial u}{\partial n} \right\} [v] d\Gamma - \epsilon \sum_{\Gamma \in \mathbf{S}} \int_{\Gamma} \left\{ \frac{\partial v}{\partial n} \right\} [u] d\Gamma + \\ \sum_{\Gamma \in \mathbf{S}} \frac{\gamma}{h} \int_{\Gamma} [u] [v] d\Gamma = l(v) \quad \forall v \in \mathcal{X}. \quad (28)$$

386 Since $[u] = 0$ on the intersections, the above formulation is consistent with (27).
 387 Furthermore, and as already stated in [75] the parameter ϵ can be set to some
 388 particular values, namely:

- 389 • For $\epsilon = +1$, the resulting method is called the symmetric interior
 390 penalty Galerkin (SIPG) method. The stiffness matrix of SIPG is sym-
 391 metric.
- 392 • If $\epsilon = 0$, we obtain the incomplete interior penalty Galerkin (IIPG)
 393 method. It involves only a few terms and is of easiest implementation.
- 394 • If $\epsilon = -1$, the resulting method is called the nonsymmetric interior
 395 penalty Galerkin (NIPG) method. It admits one unique solution and
 396 converges optimally irrespectively of the value of $\gamma > 0$.

397 For $\epsilon = 0$ and $\epsilon = +1$, the bilinear form is coercive if $\gamma > C$ and $\gamma > 2C$,
 398 respectively [75]. Similar to the stablized Lagrange multiplier method, the
 399 discontinuous Galerkin method also requires to solve an eigenvalue problem
 400 to determine the value of γ .

401 Discontinuous Galerkin method has been widely studied in various as-
 402 pects, including imposing boundary condition [45], domain decomposition
 403 [6] and contact problem [24]. In the field of Isogeometric analysis, Discon-
 404 tinuous Galerkin method has been utilized to imposing Dirichlet boundary
 405 condition for trimmed spline meshes [38]. The first article discussing discon-
 406 tinuous Galerkin method based domain decomposition strategy was written
 407 by Apostolatos *et al.* [2]. Nguyen *et al.* extended it to three-dimensional
 408 problems in [68]. Guo *et al.* [44] proposed a Nitsche's method for cou-
 409 pling Kirchhoff-Love NURBS shell patches. Since the governing equation for

Table 1: Property comparison of Lagrange multiplier, dual mortal, perturbed Lagrange multiplier, stablized Lagrange multiplier and discontinuous Galerkin methods.

Methods	well-defined	inf-sup	symmetry	positive definite	size
Lagrange multiplier	depends	depends	yes	no	enlarged
Dual mortar	yes	depends	yes	yes	reduced
Perturbed Lagrange multiplier	yes	depends	yes	no	enlarged
Stabilized Lagrange multiplier	depends	yes	yes	no	enlarged
Discontinuous Galerkin	depends	yes	depends	yes	same

Table 1: Property comparison of Lagrange multiplier, dual mortal, perturbed Lagrange multiplier, stablized Lagrange multiplier and discontinuous Galerkin methods .

410 Kirchhoff-Love shell is 4-th order PDE, C^1 continuity constraint in imposed
 411 weakly in the method.

412 Although discontinuous Galerkin method does not introduce additional
 413 DOF and does not need the judicious choice of mutiplier function space,
 414 the value of the constants in the stablizing term need to be determined.
 415 Normally, they are determined by solving a eigenvalue problem on the domain
 416 of the combination of all intersections, which leads to extra computational
 417 cost. Meanwhile, the additional stablizing terms reduce the sparsity of the
 418 global linear system. For higher order PDEs, discontinuous Galerkin method
 419 becomes more complex as higher order derivatives exists in the tractions.

420 A comparison of the variational coupling methods discussed above is
 421 shown in Table. 1.

422 3. Research Objectives

423 My dissertation research focuses on the construction of NURBS basis
 424 functions among multi-patches that are analysis-suitable for 4th order PDEs.
 425 The coupling constraints are applied weakly by using the dual mortar method.
 426 The dual basis functions are constructed based on the Bézier probjection
 427 technology proposed in [85].

428 4. Preliminaries

429 This section provides the formulation of univariate basis functions, its
 430 extention to higher dimensional space, and representations of geometries in
 431 the context of Isogeometric Analysis. For a detailed explanation we refer to.

432 4.1. Univariate B-spline basis functions

433 A univariate B-spline is piecewise polynomial curve represented as a linear
 434 combination of B-spline basis functions. Basis functions of p^{th} order B-spline
 435 with n degrees of freedom can be defined by a non-decreasing set of real
 436 numbers

$$\Xi = \{\xi_1, \xi_2, \dots, \xi_{n+p+1}\}, \quad (29)$$

which is called knot vector. B-splines that are interpolatory at the ends can be achieved by requiring the multiplicity of $p + 1$ for the first and the last knot. Associated B-spline basis functions are defined using the Cox-de Boor recursion formula:

$$N_{i,0}(\xi) = \begin{cases} 1 & \xi_i \leq \xi \leq \xi_{i+1} \\ 0 & \text{otherwise} \end{cases} \quad (30)$$

$$N_{i,p}(\xi) = \frac{\xi - \xi_i}{\xi_{i+p} - \xi_i} N_{i,p-1}(\xi) + \frac{\xi_{i+p+1} - \xi}{\xi_{i+p+1} - \xi_{i+1}} N_{i+1,p-1}(\xi) \quad (31)$$

437 4.2. Univariate NURBS basis functions

438 The univariate Non-Uniform Rational B-spline (NURBS) can describe
 439 objects that cannot be represented by polynomial basis, such as circular arcs.
 440 NURBS are built from B-splines by dividing each B-spline basis functions by
 441 a weight function

$$W(\xi) = \sum_{j=1}^n w_j N_{j,p} \quad (32)$$

442 and multiplying each B-spline basis functions by the associated weight coeffi-
 443 cient for the partition of unity. Thus, the NURBS basis functions are defined
 444 as:

$$R_{i,p}(\xi) = \frac{w_i N_{i,p}}{W(\xi)} \quad (33)$$

445 4.3. Multivariate basis functions

446 For higher dimensional spaces, the B-spline and NURBS basis functions
 447 can be formed by the Kronecker product of vectors of univariate basis func-
 448 tions. For a two-dimensional parametric space, given polynomial orders of
 449 p_ξ, p_η and degrees of freedom n_ξ, n_η in ξ, η direction, the bivariate B-spline
 450 basis functions are defined as:

$$N_{a,\mathbf{p}}(\xi, \eta) = N_{i,p_\xi}(\xi) N_{j,p_\eta}(\eta), \quad (34)$$

⁴⁵¹ where the index a is defined by the map

$$a = n_\eta i + j. \quad (35)$$

⁴⁵² The bivariate NURBS basis functions are defined as

$$R_{a,\mathbf{p}}(\xi, \eta) = \frac{w_a N_{a,\mathbf{p}}}{\sum_{i=1}^n w_i N_{i,\mathbf{p}}}, \quad (36)$$

⁴⁵³ where $n = n_\xi \times n_\eta$. With some abuse of notation, we will drop the dependency
⁴⁵⁴ on the polynomial oder and use N_i to denote both NURBS basis functions
⁴⁵⁵ and B-spline basis functions in the rest of the paper.

⁴⁵⁶ 5. Weak- C^1 coupling for two-patch planar domains

⁴⁵⁷ To ground our approach in a practical example, we consider a biharmonic
⁴⁵⁸ problem on a two-patch planar domain, as demonstrated in Figure. 4. The
⁴⁵⁹ domain Ω is decomposed to the slave subdomain Ω_s (with finer mesh on the
⁴⁶⁰ interface) and the master subdomain Ω_m (with coarser mesh on the interface).

In order of focusing on the coupling algorithm itself, we assume the boundaries that neighboring to the common intersection to be homogeneous Neumann boundaries (north and south of Ω_s and east and west of Ω_m) and the rest to be homogeneous Dirichlet boundaries (west of Ω_s and south of Ω_m), denoted by Γ_N and Γ_D respectively. Then, the strong form of the two-patch biharmonic boundary value problem writes:

$$\begin{aligned} \Delta^2 u &= f, \quad \text{in } \Omega, \\ u &= \frac{\partial u}{\partial \mathbf{n}} = 0, \quad \text{on } \Gamma_D, \\ \Delta u &= \frac{\partial \Delta u}{\partial \mathbf{n}} = 0, \quad \text{on } \Gamma_N. \end{aligned} \quad (37)$$

⁴⁶¹ 5.1. Continuity constraints

The weak solution of the biharmonic problem (37) is in the space $H^2(\Omega)$. Due to the inclusion $C^1(\Omega) \subset H^2(\Omega)$, we can use C^1 -continuous functions to approximate the solution. For the two multi-patch domain, constraints

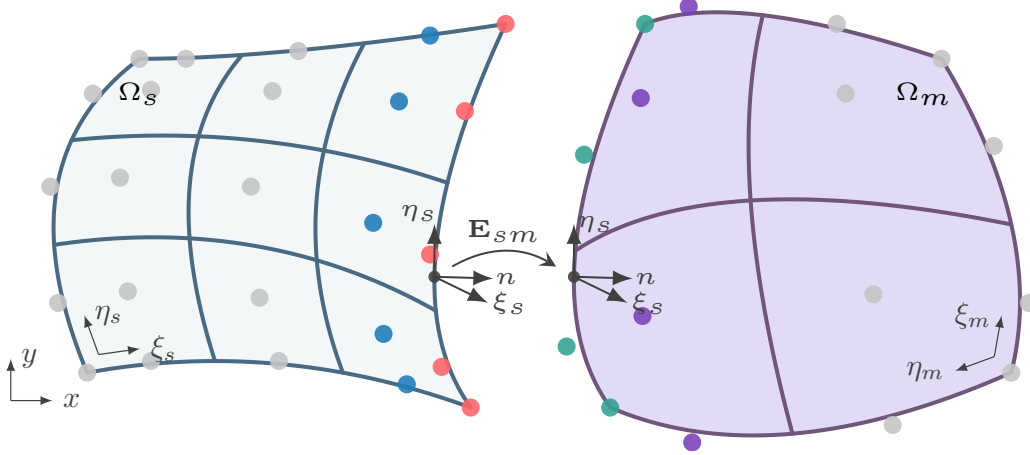


Figure 4: A two-patch planar domain constituted by Ω_m and Ω_s .

should be added to compromise the discontinuity along the intersection. In general, the following two constraints are requested for u to be C^1 -continuous

$$[u]_{\Gamma_{sm}} = 0, \quad (38a)$$

$$\left[\frac{\partial u}{\partial \mathbf{n}} \right]_{\Gamma_{sm}} = 0, \quad \text{with } \mathbf{n} = \mathbf{n}_s = -\mathbf{n}_m \quad (38b)$$

where \mathbf{n}_k is the outward normal direction of $\partial\Omega_k$.

Whereas the constraint (38a) can easily fit into the framework of dual mortar method, the constraint (39) can not be directly imposed. First of all, the existence of dual basis functions of $\frac{\partial N_i}{\partial \mathbf{n}}|_{\Gamma_{sm}}$ is doubtful. Even if they exist, as they are biorthogonal to the normal derivative of NURBS, their formulation must depend on the parameterization of Γ_{sm} , which violates the virtue of simplicity of dual basis functions. Hence, we need the following result, of which the derivatives are defined in the parametric domain and the dual basis functions can be formulated in an elegant manner.

Lemma 1. *Given two differentiable bijective geometric mappings $\mathbf{F}_s: \hat{\Omega}_s \rightarrow \Omega_s$ and $\mathbf{F}_m: \hat{\Omega}_m \rightarrow \Omega_m$, a C^0 -continuous function u is C^1 -continuous in the physical domain if and only if*

$$\left[\frac{\partial u}{\partial \xi_s} \right]_{\Gamma_{sm}} = 0 \text{ and } \left[\frac{\partial u}{\partial \eta_s} \right]_{\Gamma_{sm}} = 0. \quad (39)$$

Proof. It suffices to consider two neighboring patches as shown in Figure 4. u is C^0 -continuous function implies $\left[\frac{\partial u}{\partial \eta_s} \right]_{\Gamma_{sm}} = 0$. For the C^1 -continuity of u ,

we have the following relation

$$\begin{cases} \frac{\partial u_s}{\partial x} = \frac{\partial u_m}{\partial x} \\ \frac{\partial u_s}{\partial y} = \frac{\partial u_m}{\partial y} \end{cases} \xrightarrow{[\frac{\partial u}{\partial \eta_s}]_{\Gamma_{sm}}=0} \begin{cases} \frac{\partial u_s}{\partial \xi_s} \frac{\partial \xi_s}{\partial x} = \frac{\partial u_m}{\partial \xi_s} \frac{\partial \xi_s}{\partial x} \\ \frac{\partial u_s}{\partial \xi_s} \frac{\partial \xi_s}{\partial y} = \frac{\partial u_m}{\partial \xi_s} \frac{\partial \xi_s}{\partial y} \end{cases} \quad \text{on } \Gamma_{sm} \quad (40)$$

⁴⁷⁴ Since the geometric mapping \mathbf{F}_s is bijective, there exist an inverse mapping
⁴⁷⁵ \mathbf{F}_s^{-1} and $\det(\mathbf{F}_s^{-1}) \neq 0$. Thus, $[\frac{\partial u}{\partial \xi_s}]_{\Gamma_{sm}} = 0$. This concludes the proof. \square

The derivatives of u_m w.r.t. ξ_s and η_s can be obtained following the chain rule, as

$$\begin{bmatrix} \frac{\partial u_m}{\partial \xi_s} \\ \frac{\partial u_m}{\partial \eta_s} \end{bmatrix} = J(\mathbf{E}_{sm})^T \cdot \begin{bmatrix} \frac{\partial u_m}{\partial \xi_m} \\ \frac{\partial u_m}{\partial \eta_m} \end{bmatrix}, \quad (41)$$

⁴⁷⁶ where $J(\cdot)$ is the Jacobian of the mapping in the argument. The Jacobian of
⁴⁷⁷ the composition mapping \mathbf{E}_{sm} can be written as

$$J(\mathbf{E}_{sm}) = J((\mathbf{F}_m)^{-1} \circ \mathbf{F}_s) = J((\mathbf{F}_m)^{-1}) \cdot J(\mathbf{F}_s) = J(\mathbf{F}_m)^{-1} \cdot J(\mathbf{F}_s). \quad (42)$$

⁴⁷⁸ 5.2. Lagrange multiplier formulation and dual mortar formulation

We introduce two Lagrange multiplier spaces: M_0 is devoted to the C^0 constraint (38a) and M_1 is devoted to the C^1 constraint (39). The Lagrange multiplier formulation of the weak problem of (37) reads: find $u \in X_b$, $\lambda_0 \in M_0$ and $\lambda_1 \in M_1$ such that:

$$\begin{cases} a_b(u, v) + b_0(\lambda_0, v) + b_1(\lambda_1, v) = l(v), & \forall v \in X_b; \\ b_0(\mu_0, u) = 0, & \forall \mu_0 \in M_0; \\ b_1(\mu_1, u) = 0, & \forall \mu_1 \in M_1; \end{cases} \quad (43)$$

with

$$a_b(u, v) = \int_{\Omega} \Delta u \Delta v d\Omega, \quad (44)$$

$$b_0(\mu, u) = \int_{\Gamma_{sm}} \mu [u]_{\Gamma} d\Gamma, \quad (45)$$

$$b_1(\mu, u) = \int_{\Gamma_{sm}} \mu \left[\frac{\partial u}{\partial \xi_s} \right]_{\Gamma} d\Gamma. \quad (46)$$

⁴⁷⁹ The broken Sobolev space for the biharmonic problem is given as

$$\mathcal{X}_b := \{u \in L^2(\Omega) : u|_{\Omega_k} \in H_*^2(\Omega_k)\}, \quad (47)$$

480 with

$$H_*^2(\Omega_k) := \left\{ u \in H^2(\Omega_k) : u = 0 \text{ and } \frac{\partial u}{\partial \mathbf{n}} = 0 \text{ on } \partial\Gamma_D \cap \partial\Omega_k \right\}. \quad (48)$$

481 By moving the constraints from the problem statement to the definition of the
482 trial and test function spaces, we obtain the following variational problem:
483 find $u \in \mathcal{K}_b$, such that

$$a_b(u, v) = l(v), \quad \forall v \in \mathcal{K}_b, \quad (49)$$

484 where

$$\mathcal{K}_b := \{u \in \mathcal{X}_b : b_0(u, \mu_0) = 0 \text{ and } b_1(u, \mu_1) = 0 \quad \forall (\mu_0, \mu_1) \in \mathcal{M}_0 \times \mathcal{M}_1\}. \quad (50)$$

485 On one hand, the absence of the Lagrange multipliers λ_0 and λ_1 reduces the
486 size of the discretized problem and recovers the symmetric positive definite
487 structure of the stiffness matrix. As a result, efficient iterative solvers can be
488 applied for the problem. On the other hand, in the standard formalism, \mathcal{M}_0
489 and \mathcal{M}_1 are discretized by the trace of one side of the intersection so that
490 the construction of \mathcal{K}_b^h requires a factorization of a global constraint matrix,
491 which is not a trivial task.

492 However, in the following section, we will show that, with the help of dual
493 basis functions, the discretized function space \mathcal{K}_b^h can be formulated in an
494 elegant manner.

495 5.3. Finite element approximation

496 Suppose that $\mathcal{X}_b^h \subset \mathcal{X}_b$, $\mathcal{M}_0^h \subset \mathcal{M}_0$ and $\mathcal{M}_1^h \subset \mathcal{M}_1$ are finite-dimensional
497 linear subspaces of the Hilbert spaces \mathcal{X}_b , \mathcal{M}_0 , and \mathcal{M}_1 ; we study the finite
498 element approximation of the abstract problem (43).

Assumption 1. All bilinear functionals are bounded; i.e., there exist positive constants C_a , C_{b_0} and C_{b_1} such that

$$\begin{aligned} |a_b(u, v)| &\leq C_a \|u\|_{H^2} \|v\|_{H^2} & \forall u, v \in \mathcal{X}_b \\ |b_0(\mu_0, u)| &\leq C_{b_0} \|\mu_0\|_{L^2} \|u\|_{H^2} & \forall \mu_0 \in \mathcal{M}_0, u \in \mathcal{X}_b \\ |b_1(\mu_1, u)| &\leq C_{b_1} \|\mu_1\|_{L^2} \|u\|_{H^2} & \forall \mu_1 \in \mathcal{M}_1, u \in \mathcal{X}_b \end{aligned} \quad (51)$$

499 **Assumption 2.** In addition, we assume that the bilinear functional $a_b(\cdot, \cdot)$
500 is coercive on \mathcal{K}_b , i.e.,

$$\exists c_a > 0 \quad s.t. \quad \forall v^h \in \mathcal{K}_b^h, \quad a_b(v^h, v^h) \geq c_a \|v^h\|_{H^2} \quad (52)$$

501 Following standard techniques [20], we now obtain a bound on the error
 502 between u and u^h in term of the best approximation errors, which can be
 503 considered as Céa's lemma for mixed problems.

504 **Theorem 1.** *Under the above assumptions, there exists a unique solution
 505 $u^h \in \mathcal{K}_b^h$ satisfies (49). Furthermore,*

$$\|u - u^h\|_{H^2} \leq \left(1 + \frac{C_a}{c_a}\right) \inf_{v^h \in \mathcal{K}_b^h} \|u - v^h\|_{H^2} + \frac{C_{b_0}}{c_a} \inf_{\mu_0^h \in \mathcal{M}_0^h} \|\lambda_0 - \mu_0^h\|_{L^2} + \frac{C_{b_1}}{c_a} \inf_{\mu_1^h \in \mathcal{M}_1^h} \|\lambda_1 - \mu_1^h\|_{L^2} \quad (53)$$

506 Hence, the error of finite element approximations in broken $H^2(\Omega)$ norm
 507 are bounded by the best approximation error of $v^h \in \mathcal{K}_b^h$ in broken $H^2(\Omega)$
 508 norm and $\mu_0^h \in \mathcal{M}_0^h$, $\mu_1^h \in \mathcal{M}_1^h$ in $L^2(\Gamma)$ norm. In general, the approximation
 509 ability of p^{th} order piecewise polynomial in \mathcal{X}_b^h is given by

$$\|u - u^h\|_{H^2} \leq Ch^{p-1}. \quad (54)$$

510 where C is a constant that is independent of the mesh size h . However, the
 511 optimality of $u^h \in \mathcal{K}_b^h$ requires the *inf-sup* stability of bilinear functional b_0
 512 and b_1 . The analytical study of the *inf-sup* stability is beyond the scope
 513 of this paper. Instead, we demonstrate the approximation ability of \mathcal{K}_b^h by
 514 directly conducting H^2 projection in different numerical examples.

515 Meanwhile, the approximation ability of the Lagrange multiplier spaces
 516 \mathcal{M}_0^h and \mathcal{M}_1^h also influence the optimality of the finite element approxima-
 517 tion. Whereas u is approximated in H^2 space, λ_0 and λ_1 are approximated in
 518 L^2 space. Hence, the optimality of the finite element approximation requires
 519 that both \mathcal{M}_0^h and \mathcal{M}_1^h are at least $p - 2$ complete, i.e., functions in \mathcal{M}_0^h and
 520 \mathcal{M}_1^h can exactly represent polynomials up to order $p - 2$.

521 5.4. Discretization

In order to approximate the solution of the variational problem, we use the NURBS basis functions $N_i^{(s)}$ $i \in I_s$ and $N_j^{(m)}$ $j \in I_m$ to discretize coupled patches Ω_s and Ω_m , respectively. An appropriate offset has been made so that there is no overlapping between index sets I_s and I_m (given n_s basis functions in Ω_s , we can assume the starting index in the index set I_m is

$n_s + 1$). The discretized geometrical mappings are represented by

$$\mathbf{F}_s = \sum_{i \in I_s} \mathbf{P}_i^s N_i^s, \quad (55)$$

$$\mathbf{F}_m = \sum_{i \in I_m} \mathbf{P}_i^m N_i^m, \quad (56)$$

where the control points $\mathbf{P}_i^s, \mathbf{P}_i^m \in \mathbb{R}^2$. The same basis functions are also used to discretize the test function u in broken Sobolev space \mathcal{X}_b , as

$$u^h = \sum_{i \in I_s + I_m} U_i N_i, \quad (57)$$

with

$$N_i = \begin{cases} N_i^s, & i \in I_s; \\ N_i^m, & i \in I_m. \end{cases} \quad (58)$$

As compared to the standard formalism that utilizes the trace of the slave patch on the intersection as the discretization of Lagrange multipliers, in this research, we construct Lagrange multipliers by using Bézier dual basis. We first classify NURBS basis functions into five different kinds, as shown in Figure. 4, namely:

1. The basis functions $N_i^{(s)}$ such that $\text{supp}(N_i^{(s)}) \cap \Gamma_{sm} = \emptyset$ and $\text{supp}(\frac{\partial N_i^{(s)}}{\partial \xi_s}) \cap \Gamma_{sm} \neq \emptyset$, whose indices are in the index set I_i . (denoted by blue dots)
2. The basis functions $N_i^{(s)}$ such that $\text{supp}(N_i^{(s)}) \cap \Gamma_{sm} \neq \emptyset$, whose indices are in the index set I_{ii} . (denoted by red dots)
3. The basis functions $N_i^{(m)}$ such that $\text{supp}(N_i^{(m)}) \cap \Gamma_{sm} = \emptyset$ and $\text{supp}(\frac{\partial N_i^{(m)}}{\partial \xi_s}) \cap \Gamma_{sm} \neq \emptyset$, whose indices are in the index set I_{iii} . (denoted by green dots)
4. The basis functions $N_i^{(m)}$ such that $\text{supp}(N_i^{(m)}) \cap \Gamma_{sm} \neq \emptyset$, whose indices are in the index set I_{iv} . (denoted by purple dots)
5. All basis functions neither the supports of themselves nor the supports of their first order derivatives in ξ_s direction intersect with Γ_{sm} , whose indices are in the index set I_v . (denoted by grey dots)

For the basis functions of the second kind, their restrictions on the intersection Γ_{sm} are one dimensional NURBS basis functions $N_{i,p_\eta}^{(s)} i \in \{1, 2, \dots, n_\eta^s\}$ that are used to discretize the tensor-product domain Ω_s in η direction. In

order to obtain an Identity matrix on the slave side of the discretized bilinear form b_0 , the associated dual basis functions of $N_{i,p_\eta}^{(s)}$ are used to discretize the Lagrange multiplier space \mathcal{M}_0 , as

$$\lambda_0^h = \sum_{i=1}^{n_\eta^s} \Lambda_i^0 \hat{N}_{i,p_\eta}^{(s)}. \quad (59)$$

For the basis functions of the first kind, the restrictions of their first order derivatives on the intersection Γ_{sm} can be written as $c N_{i,p_\eta}^{(s)} i \in \{1, 2, \dots, n_\eta^s\}$, with $c = N_{n_\xi^s - 1, p_\xi}^{(s)}(1)$. Hence, the Lagrange multiplier space \mathcal{M}_1 can be discretized by

$$\lambda_1^h = \sum_{i=1}^{n_\eta^s} \Lambda_i^1 \tilde{N}_i, \quad \text{with } \tilde{N}_i = \frac{1}{c} N_{i,p_\eta}^{(s)}. \quad (60)$$

We denote the basis functions in \mathcal{M}_0^h and \mathcal{M}_1^h as the dual basis functions of the second and the first kinds of NURBS basis functions, respectively.

By substituting these NURBS approximations into the Lagrange multiplier formulation (43), we obtain the following linear system:

$$\begin{bmatrix} \mathbf{K} & \mathbf{B}^T \\ \mathbf{B} & \mathbf{0} \end{bmatrix} \begin{bmatrix} \mathbf{U} \\ \boldsymbol{\Lambda}_0 \\ \boldsymbol{\Lambda}_1 \end{bmatrix} = \begin{bmatrix} \mathbf{F} \\ \mathbf{0} \end{bmatrix}, \quad (61)$$

where \mathbf{K} and \mathbf{F} are the stiffness matrix and the load vector for the uncoupled problem, respectively. \mathbf{B} is the constraint matrix discretized from the bilinear forms b_0 and b_1 . In order to construct the finite element space \mathcal{K}_b^h , we need to solve the constraint matrix \mathbf{B} 's null space $\mathbf{C} = \ker(\mathbf{B})$. Since the structure of the constraint matrix \mathbf{B} depends on the index sets I_s and I_m and the ordering of Lagrange multiplier basis functions, without adding any constraints on the indices, we introduce two permutation matrices \mathbf{P}_c and \mathbf{P}_r (this step is not necessary from the implementation point of view, but is very convenient for the demonstration, especially for multi-patch problem). We define the column permutation matrix \mathbf{P}_c as

$$\begin{bmatrix} \mathbf{I}_i \\ \mathbf{I}_{ii} \\ \mathbf{I}_{iii} \\ \mathbf{I}_{iv} \\ \mathbf{I}_v \end{bmatrix} = \mathbf{P}_c \begin{bmatrix} \mathbf{I}_s \\ \mathbf{I}_m \end{bmatrix}, \quad (62)$$

564 where \mathbf{I}_i is the vector form of the index set I_i . For an appropriate row
 565 permutation matrix \mathbf{P}_r , the modified constraint matrix can be written in a
 566 partitioned form as

$$\mathbf{B}_p = \mathbf{P}_r \mathbf{B} \mathbf{P}_c^T = \begin{bmatrix} \mathbf{B}_1^1 & \mathbf{B}_1^2 & \mathbf{B}_1^3 & \mathbf{B}_1^4 & \mathbf{0} \\ \mathbf{0} & \mathbf{B}_2^2 & \mathbf{B}_2^3 & \mathbf{0} & \mathbf{0} \end{bmatrix}, \quad (63)$$

567 where \mathbf{B}_i^j corresponds to the contribution of the inner product of the basis
 568 functions of the j^{th} kind with the dual basis functions of the i^{th} kind. \mathbf{P}_r
 569 can be defined as a row permutation matrix such that the resulted block
 570 sub-matrices \mathbf{B}_1^1 and \mathbf{B}_2^2 are both identity matrices. Under a rank-preserving
 571 transformation \mathbf{T} , we can eliminate the block sub-matrix \mathbf{B}_1^2 , as

$$\mathbf{T}\mathbf{B}_p = \begin{bmatrix} & \mathbf{I} & \mathbf{B}_1^3 - \mathbf{B}_1^2\mathbf{B}_2^3 & \mathbf{B}_1^4 & \mathbf{0} \\ & & \mathbf{B}_2^3 & \mathbf{0} & \mathbf{0} \end{bmatrix}. \quad (64)$$

572 We may now take

$$\mathbf{C}_p := \ker(\mathbf{B}_p) = \begin{bmatrix} \mathbf{B}_1^2\mathbf{B}_2^3 - \mathbf{B}_1^3 & -\mathbf{B}_1^4 & \mathbf{0} \\ -\mathbf{B}_2^3 & \mathbf{0} & \mathbf{0} \\ & & \mathbf{I} \end{bmatrix}. \quad (65)$$

573 Hence, the null space of \mathbf{B} can be taken as

$$\mathbf{C} = \mathbf{P}_c^T \mathbf{C}_p. \quad (66)$$

574 Now we can discretize functions in \mathcal{K}_b^h as

$$u^h = \mathbf{N}^T \mathbf{U}, \quad \text{with } \mathbf{U} = \mathbf{C} \tilde{\mathbf{U}}, \quad (67)$$

575 where \mathbf{N} is the vector form of basis functions of \mathcal{X}_b^h , and $\tilde{\mathbf{U}}$ is the control
 576 point vector. By substituting the above discretization in the weak form (50),
 577 we obtain the following linear system to be solved:

$$\mathbf{C}^T \mathbf{K} \mathbf{C} \tilde{\mathbf{U}} = \mathbf{C}^T \mathbf{F}. \quad (68)$$

578 Because of the biorthogonality of the NURBS basis functions and their dual
 579 basis functions, the constrained solution spcae \mathcal{K}_b^h can be constructed very
 580 efficiently, leading to a sparse, symmetric positive definite formulation.

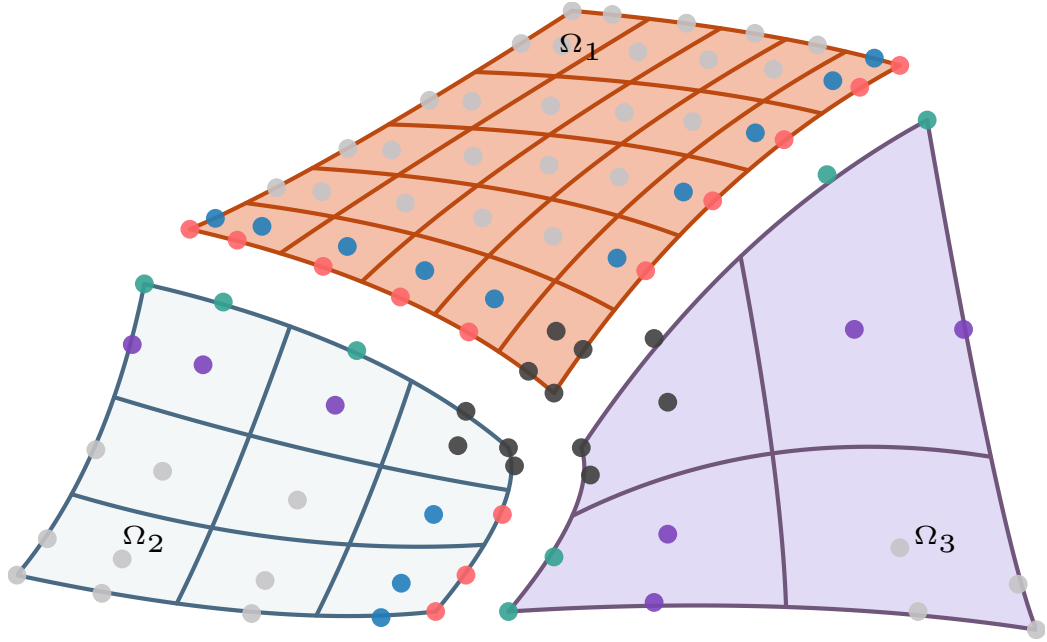


Figure 5: A three-patch planar domain constituted by Ω_1 , Ω_2 and Ω_3 .

581 6. Weak- C^1 coupling for multi-patch planar domains

582 To generate complex geometries, we need to decompose domain to mul-
 583 tiple patches. Unfortunately, we cannot apply directly the results of two-
 584 patch coupling to this more general mortar situation. The main issue is
 585 the so-called cross points. For a multi-patch decomposition, at least three
 586 subdomains meet at an interior crosspoint and several interfaces can share
 587 this cross point as a common endpoint (Figure. 5). If we use the discretized
 588 Lagrange multipliers proposed in the previous section, owing to the presence
 589 of cross points, some of the control points will serve as both slave points
 590 (indices in I_1 and I_2) and master points (indices in I_3 and I_4). Hence, there
 591 is no permutation matrices such that the constraint matrix \mathbf{B} can be mod-
 592 ified to the form as equation (64), of which the null space can be found in
 593 a trivial way. Even more, although the constraint matrices defined on each
 594 interfaces are full row rank, the assembled constraint matrix \mathbf{B} may not be
 595 full row rank in most cases, which renders the linear system (61) to be rank
 596 deficient. As a result, either modifications to the Lagrange multipliers or to
 597 the method itself is required so that the proposed method can be generalized
 598 to a setting where a domain can be decomposed to an arbitrary number of

599 patches. Before we start this section, we would like to introduce the sixth
600 kind of NURBS basis function that associated with the cross point v , as

601 6. The basis function N_i such that $\text{supp}(N_i) \cap v \neq 0$, or $\text{supp}(\frac{\partial N_i}{\partial \xi}) \cap v \neq$
602 0, or $\text{supp}(\frac{\partial N_i}{\partial \eta}) \cap v \neq 0$ or $\text{supp}(\frac{\partial^2 N_i}{\partial \xi \partial \eta}) \cap v \neq 0$, whose indices are in the
603 index set I_{vi} . (denoted by black dots in Figure. 5)

604 The rest five kinds of NURBS basis function remain the same except their
605 intersection with the sixth kind are excluded, that is

$$I_k = I_k - I_{vi} \cap I_k, \quad k \in \{i, ii, \dots, v\}. \quad (69)$$

606 The basis functions in \mathcal{M}_0^h and \mathcal{M}_1^h can be classified as the dual basis func-
607 tions of the NURBS basis function of the 1st, 2nd and 6th kind, respectively.
608 The domains on the two sides of each interface can still be considered as slave
609 and master based on the same rule as for the two-patch coupling case.

610 6.1. Cross point modification

611 Since using the discretization of Lagrange multipliers proposed for two-
612 patch coupling case directly results in over-constrained constraint matrix \mathbf{B}
613 for the control points round the crosspoints, we can remedy this issue by re-
614 ducing the dimension of the Lagrange multiplier spaces. Roughly speaking,
615 we have to remove the two degrees of freedom of the Lagrange multiplier
616 spaces associated with each cross point so that the resulted Lagrange mul-
617 plier spaces on each interface should have the same dimension as $\mathcal{X}_b^h|_{\Omega_s} \cap H_0^2(\Gamma_{sm})$.

618 This can be achieved by two ways: we can either coarse the mesh for the
619 Lagrange multiplier in the neighborhood of the cross point, or reduce their
620 polynomial degree in the neighborhood of the cross point. An example for
621 quadratic 1-D B-spline basis functions is shown in Figure. 6. The coarsened
622 basis functions are achieved by replacing the first three and last three basis
623 functions by their summations, while we can construct degree reduced basis
624 functions by reduce the polynomial degree of the first and last two elements
625 by one while retaining the inter-element continuity.

626 Although the degree reduction is not a trivial task for dual basis, the
627 summation trick can be applied to coarse dual basis functions. After the
628 coarsen procedure, the dual basis functions associated with the basis func-
629 tions of 6th kind are all eliminated so that no inter-dependencies will happen

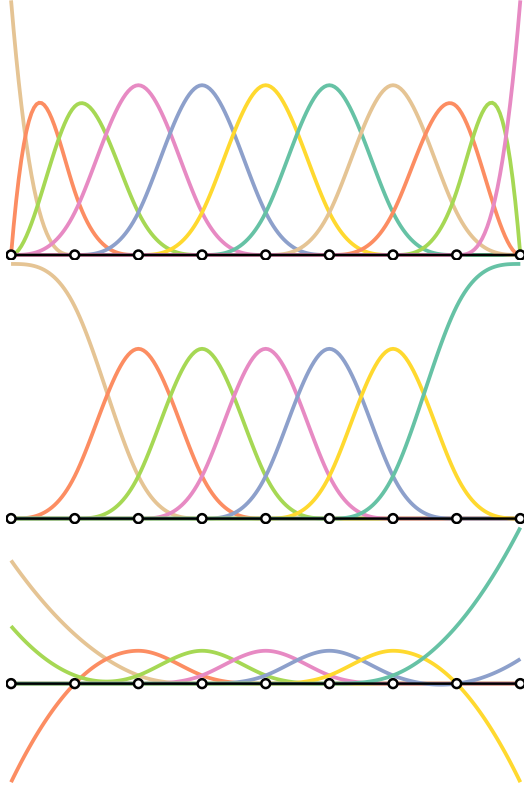


Figure 6: Quadratic basis functions and their cross point modifications. Top: original quadratic basis functions. Middle: coarsened basis functions. Bottom: degree reduced basis functions

in the neighborhood of the cross point. We can define a column permutation matrix

$$\begin{bmatrix} \mathbf{I}_i \\ \mathbf{I}_{ii} \\ \mathbf{I}_{iii} \\ \mathbf{I}_{iv} \\ \mathbf{I}_{vi} \\ \mathbf{I}_v \end{bmatrix} = \tilde{\mathbf{P}}_c \begin{bmatrix} \mathbf{I}_1 \\ \mathbf{I}_2 \\ \mathbf{I}_3 \end{bmatrix}. \quad (70)$$

With a suitable row permutation matrix $\tilde{\mathbf{P}}_r$, the constraint matrix \mathbf{B} can be modified as

$$\tilde{\mathbf{B}}_p := \tilde{\mathbf{P}}_r \mathbf{B} \tilde{\mathbf{P}}_c^T = \begin{bmatrix} \mathbf{B}_1^1 & \mathbf{B}_1^2 & \mathbf{B}_1^3 & \mathbf{B}_1^4 & \mathbf{B}_1^6 & \mathbf{0} \\ \mathbf{0} & \mathbf{B}_2^2 & \mathbf{B}_2^3 & \mathbf{0} & \mathbf{B}_2^6 & \mathbf{0} \end{bmatrix}, \quad (71)$$

634 with \mathbf{B}_1^1 and \mathbf{B}_2^2 be identity matrices. Hence, its null space can be found as

$$\tilde{\mathbf{C}}_p := \ker(\tilde{\mathbf{B}}_p) = \begin{bmatrix} \mathbf{B}_1^2 \mathbf{B}_2^3 - \mathbf{B}_1^3 & -\mathbf{B}_1^4 & -\mathbf{B}_1^6 & \mathbf{0} \\ -\mathbf{B}_2^3 & \mathbf{0} & -\mathbf{B}_2^6 & \mathbf{0} \\ \vdots & \vdots & \vdots & \vdots \\ \mathbf{I} & & & \end{bmatrix}. \quad (72)$$

635 Although the boundary modification by coarsening eliminates the inter-dependency
636 in the neighborhood of cross points, numerical tests demonstrate sub-optimality.

637 6.2. Explicitly solve the null space

638 Instead of modifying the Lagrange multipliers, we can solve the null space
639 of the over-constrained constraint matrix \mathbf{B} directly. Seveal matrix factoriza-
640 tion methods can be used to solve the null space, including LU, QR, SVD. For
641 example, a rank-revealing QR factorization over a rank-deficiency constraint
642 matrix \mathbf{B} yields

$$\mathbf{BP} = \mathbf{Q} \begin{bmatrix} \mathbf{R}_1 & \mathbf{R}_2 \\ \mathbf{0} & \mathbf{0} \end{bmatrix} \quad (73)$$

643 where \mathbf{P} is a permutation matrix, \mathbf{Q} is an unitary matrix, \mathbf{R}_1 is a upper
644 triangular matrix and \mathbf{R}_2 is a rectangular matrix. The null space can be
645 taken as

$$\ker(\mathbf{B}) = \mathbf{P} \begin{bmatrix} -\mathbf{R}_1^{-1} \mathbf{R}_2 \\ \mathbf{I} \end{bmatrix}. \quad (74)$$

646 However, this requires a factorization of the entire constraint matrix \mathbf{B} and
647 we fail to utilize the advantage of the Bézier dual basis. Even more, the
648 sparsity of the constrained stiffness matrix might be impacted as the inverse
649 of \mathbf{R}_1 is a dense matrix. This type of global factorization has been utilized
650 for patch coupling problem in [27, 28, 32].

651 Instead of solving the null space directly, we will localize the constraint
652 to each cross point and solve the null space of a localized linear system. For
653 the constraint matrix \mathbf{B} constructed by the Lagrange multipliers without
654 modification, we assume there exist a row permutation matrix $\hat{\mathbf{P}}_r$ such that

$$\hat{\mathbf{B}}_p := \hat{\mathbf{P}}_r \mathbf{B} \hat{\mathbf{P}}_c^T = \begin{bmatrix} \mathbf{B}_1 \\ \mathbf{B}_2 \end{bmatrix} = \begin{bmatrix} \mathbf{B}_6^1 & \mathbf{B}_6^2 & \mathbf{B}_6^3 & \mathbf{B}_6^4 & \mathbf{B}_6^6 & \mathbf{0} \\ \bar{\mathbf{B}}_1^1 & \bar{\mathbf{B}}_1^2 & \bar{\mathbf{B}}_1^3 & \bar{\mathbf{B}}_1^4 & \bar{\mathbf{B}}_1^6 & \mathbf{0} \\ \mathbf{0} & \mathbf{B}_2^2 & \mathbf{B}_2^3 & \mathbf{0} & \mathbf{B}_2^6 & \mathbf{0} \end{bmatrix}, \quad (75)$$

655 with \mathbf{B}_1^1 and \mathbf{B}_2^2 be identity matrices. \mathbf{B}_1 consists of constraints relevant to
656 cross point while \mathbf{B}_2 consists of constraints relevant to intersections.

657 The null space of \mathbf{B}_2 can be found as

$$\mathbf{C}_2 := \ker(\mathbf{B}_2) = \begin{bmatrix} \mathbf{B}_1^2 \mathbf{B}_2^3 - \mathbf{B}_1^3 & -\mathbf{B}_1^4 & -\mathbf{B}_1^6 & \mathbf{0} \\ -\mathbf{B}_2^3 & \mathbf{0} & -\mathbf{B}_2^6 & \mathbf{0} \\ \vdots & & \vdots & \\ \mathbf{I} & & & \end{bmatrix}. \quad (76)$$

Due to the inclusion $\hat{\mathbf{C}}_p := \ker(\hat{\mathbf{B}}_p) \subset \ker(\mathbf{B}_2)$, we can construct $\hat{\mathbf{C}}_p$ by

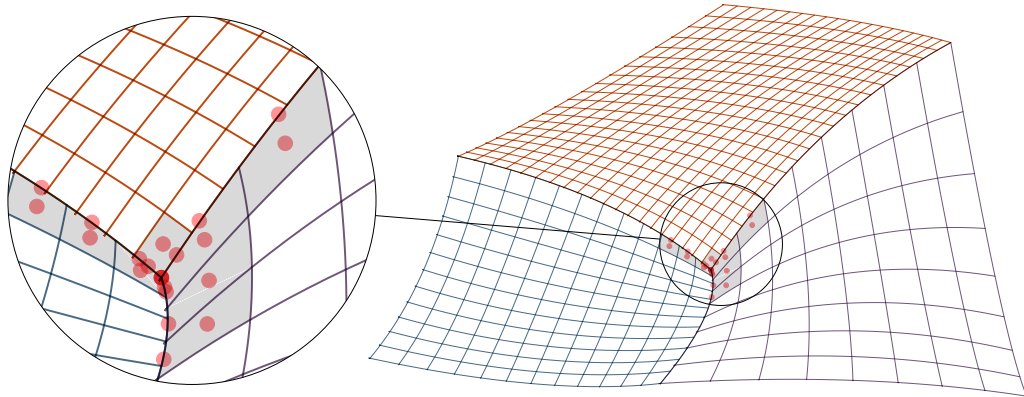


Figure 7: Control points (red) involved in crosspoint constraints (\mathbf{B}_1).

solving $\ker(\mathbf{B}_1 \mathbf{C}_2)$. Since dual basis functions have compact support, \mathbf{B}_1 and \mathbf{C}_2 are all sparse matrices (control points involved in \mathbf{B}_1 are demonstrated in Figure. 7). We can split the columns of \mathbf{C}_2 into two matrices, as

$$\begin{aligned} \mathbf{C}_2^1 &:= \{v \in \mathbf{C}_2 : \mathbf{B}_1 v \neq 0\}, \\ \mathbf{C}_2^2 &:= \{v \in \mathbf{C}_2 : \mathbf{B}_1 v = 0\}. \end{aligned} \quad (77)$$

658 Such a split can be defined a priori, based on the discretization of each patch.
 659 A demonstration of the split is given in Figure. 8. Note that $\mathbf{C}_2^2 \subset \hat{\mathbf{C}}_p$, $\hat{\mathbf{C}}_p$
 660 can be written as

$$\hat{\mathbf{C}}_p = [\mathbf{C}_2^1 \ker(\bar{\mathbf{B}}_p) \quad \mathbf{C}_2^2], \text{ with } \bar{\mathbf{B}}_p = \mathbf{B}_1 \mathbf{C}_2^1. \quad (78)$$

661 Compared with the constraint matrix \mathbf{B} whose size increases as we refine
 662 the mesh, the row size of $\bar{\mathbf{B}}_p$ is fixed and its column size is fixed after certain
 663 refinement. A comparison of the size of matrix \mathbf{B} and matrix $\bar{\mathbf{B}}_p$ as a function

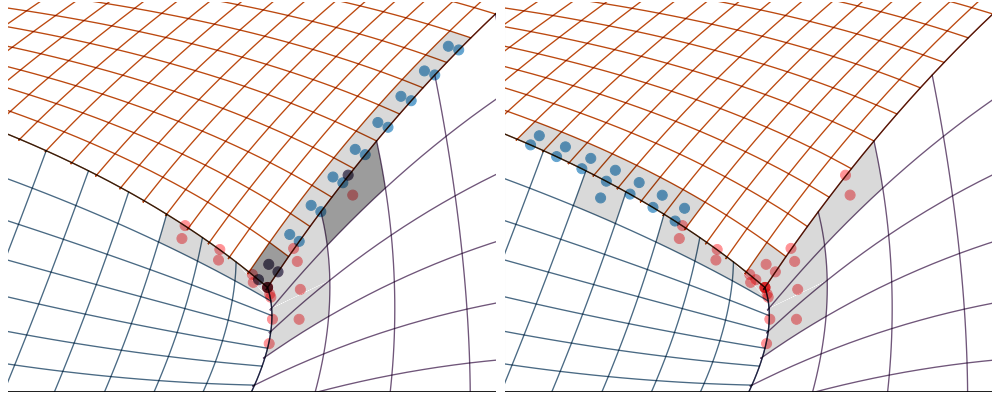


Figure 8: Control points of basis functions (blue) defined by columns of \mathbf{C}_2 . Left: Basis classified to \mathbf{C}_2^1 ; Right: Basis classified to \mathbf{C}_2^2

of the degrees of freedom is given in Figure. 9 for the three-patch coupling in Figure. 5 with 2nd order B-spline basis functions. As can be seen, the size of \mathbf{B} grows rapidly as the mesh being refined. The computational cost of directly solving its kernel will be very expensive. However, owing to the compact support of dual basis function, we can transfer a global, size-varying problem (factorization on \mathbf{B}) to a local, size-fixed problem (factorization on $\bar{\mathbf{B}}_p$), and the problem size is very small (12×24 for this case).

A graphical comparison of the sparsity patterns among standard Lagrange multiplier with global factorization, Bézier dual basis with global factorization and Bézier dual basis with local factorization is given in Figure. 10. As expected, the standard method yields the lowest sparsity, while Bézier dual basis with local factorization yields the highest sparsity (40% sparser). Meanwhile, the Bézier dual basis does not significantly improve the sparsity if a global factorization is applied to construct \mathcal{K}_b^h . Moreover, a global factorization yeilds entries with very small absolute values ($\leq 10^{-14}$), especially for the constraint matrix formed by Bézier dual basis, while all entries are away from zero for the local factorization.

7. Numerical results

All our numerical results are obtained via an in-house C++ code.

7.1. A numerical study of the completeness of Bézier dual basis

We consider the completeness of Bézier dual basis on the one dimensional domain, $\Omega = (0, 1)$. The domain Ω is uniformly partitioned into two elements,

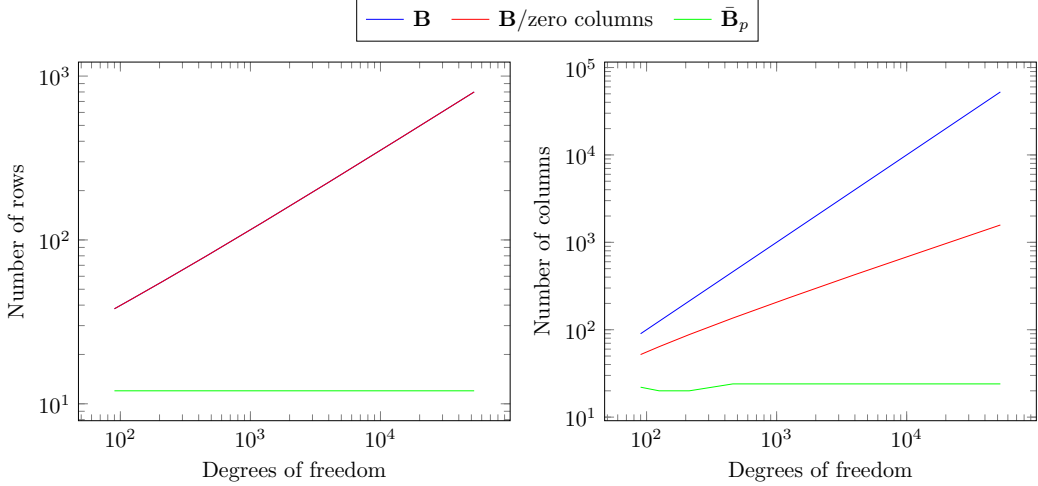


Figure 9: The change of matrix size of \mathbf{B} , \mathbf{B} with zero columns being removed, and $\bar{\mathbf{B}}_p$, as a function of the degrees of freedom. The constraint matrix \mathbf{B} is formulated for the three-patch coupling in Figure. 5 with 2nd order B-spline basis functions.

since the Bézier dual basis is equivalent to the global dual basis on one element domain. In the numerical test, we find the L^2 approximation of n^{th} order Legendre polynomial in the Bézier dual space, as Legendre polynomials are orthogonal to each other.

The test results are disappointed, the Bézier dual basis of arbitrary order is only complete for zeroth order polynomial i.e., only the error of the L^2 projection of constant function is below the round-off error. The results of projecting Legendre polynomials up to 3rd order onto 3rd order Bézier dual basis are demonstrated in Fig. 11. As can be seen, there are huge discrepancies between the approximations and original functions for all Legendre polynomials except constant. In other words, the L^2 approximation of Bézier dual basis is only of first-order, which might deteriorate the optimality of the finite element approximation.

In the finite element context, the construction of dual basis that can reproduce polynomial of degree $p - 1$ is thoroughly studied in [70]. However, the construction procedure is complicated and gets even worse for higher inter-element continuity. Following this approach, a $p - 1$ complete dual basis function for a quadratic B-spline basis function was constructed in [21], but its support is much larger than its B-spline counterpart. On the other side, though the poor polynomial completeness, Bézier dual basis can be

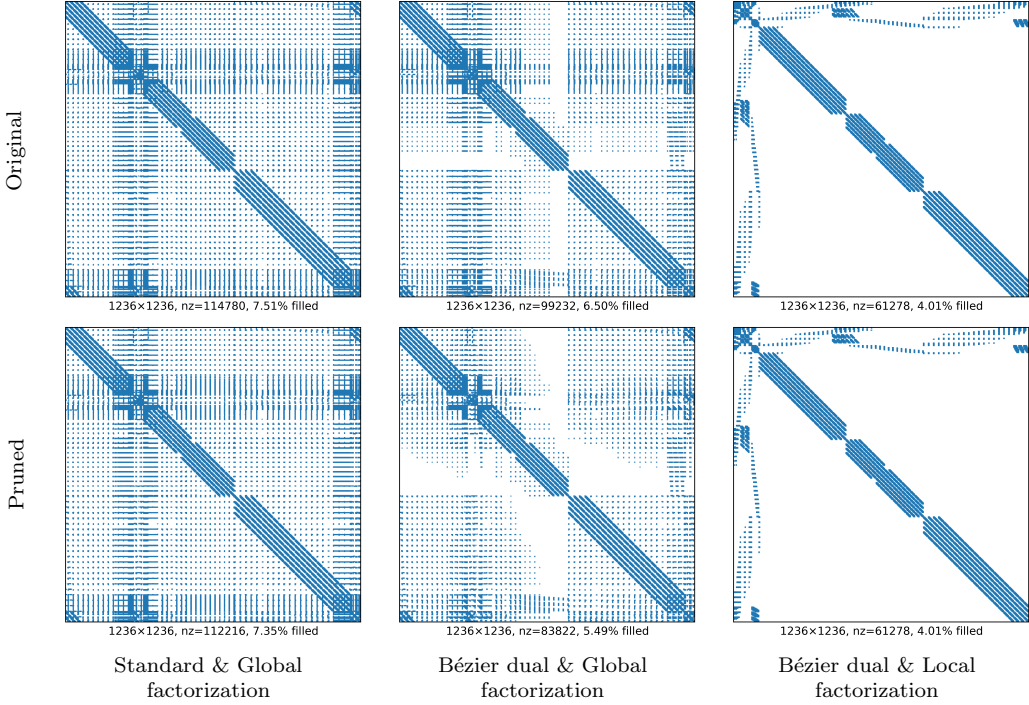


Figure 10: Sparsity patterns of constrained stiffness matrices. Left: standard Lagrange multipliers with global factorization. Middle: Bézier dual basis with global factorization. Right: Bézier dual basis with localized factorization. Top: original matrix. Bottom: small absolute values ($\leq 10^{-14}$) be pruned. All stiffness matrices are formulated for the three-patch coupling in Figure. 5 with 3rd order B-spline basis functions after 4 refinements. The number of non-zero entries is given by nz.

706 constructed in a straightforward manner, without solving additional linear
 707 system. Hence, in the rest examples, we will testify the performance of C^1
 708 dual mortaring and the influence of the Bézier dual basis on the optimality
 709 of the finite element approximation.

710 *7.2. Biharmonic problem on a two-patch domain with homogeneous Dirichlet
 711 Boundary*

712 We first solve a biharmonic problem $\Delta^2 u = f$ on a square domain $\Omega =$
 713 $(0, 1) \times (0, 1)$. The manufactured solution is given as

$$u(x, y) = \sin(3\pi x)^2 \sin(3\pi y)^2, \quad (79)$$

714 which satisfies the homogeneous Dirichlet boundary condition ($u = \frac{\partial u}{\partial n} =$
 715 0) and is visualized in Figure. 12. The domain Ω is decomposed into two

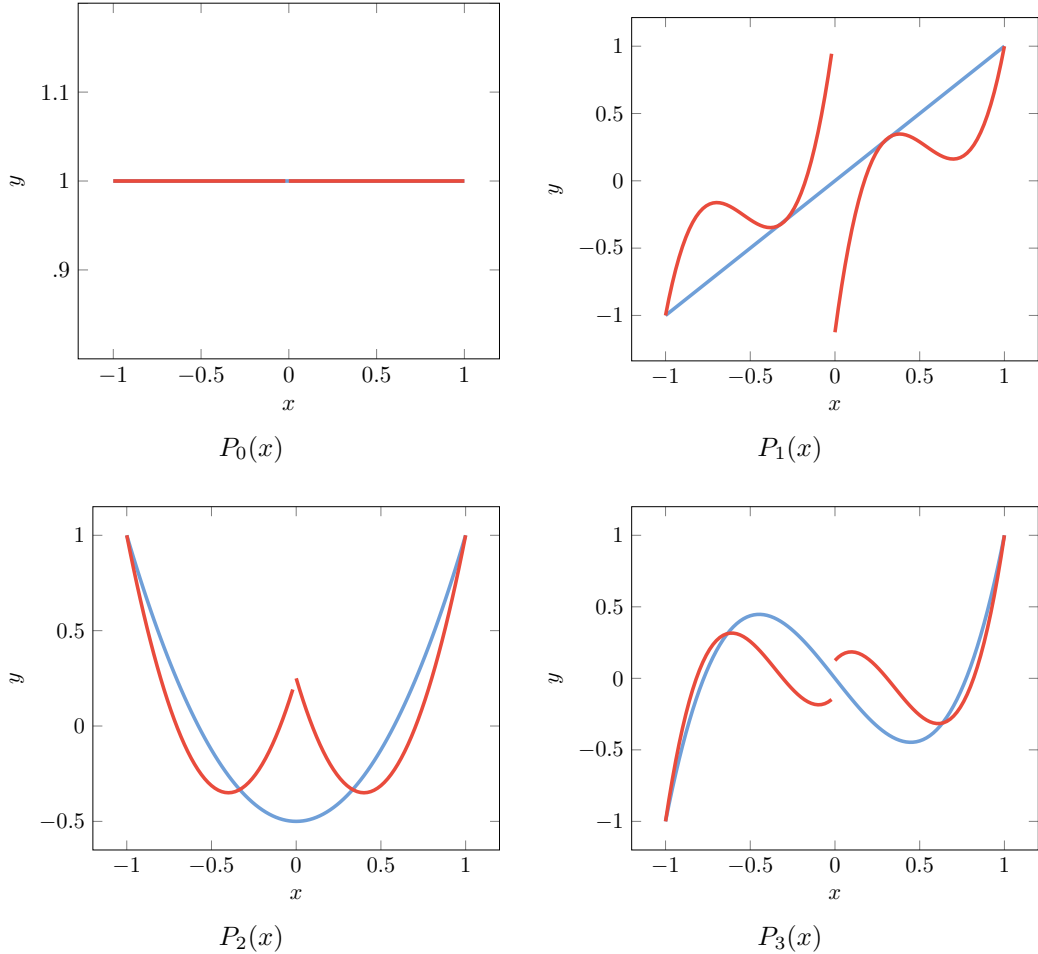


Figure 11: The Legendre polynomials (—) and their approximations (—) in 3^{rd} order Bézier dual space composed of two elements. Bézier dual basis cannot duplicate all except the constant function.

716 patches, namely $\Omega_1 = (0, 0.4) \times (0, 1)$ and $\Omega_2 = (0.4, 1) \times (0, 1)$, as shown in
 717 Figure. 12a. The right-hand side function f can be obtained by applying the
 718 biharmonic operator to u .

719 We conduct convergence studies for $p = 2, 3, 4, 5$ in both L^2 norm and
 720 H^2 norm, as shown in Fig. 13. However, though the theoretical flaw of
 721 Bézier dual basis, its performances in real problem are surprisingly well. As
 722 can be seen, both global dual basis and Bézier dual basis obtain optimal
 723 convergence rate in both norm measures for all polynomial degrees (The op-
 724 timal convergence rate for $p = 2$ in L^2 norm is 2, which can be testified by
 725 Aubin-Nitsche duality argument[][],). One conjecture can be made is that
 726 for biharmonic problems, the coefficients of the best approximation error of
 727 Lagrange multipliers are very small so that their contribution in the finite el-
 728 ement approximation error can be ignored. Moreover, the accuracy of Bézier
 729 dual basis are higher than that of global dual basis with the same refinement
 730 level.

731 To study the performance of proposed methods in detail, we consider
 732 extreme conditions e.g. distorted mesh (Figure. 12b), mismatched mesh
 733 (Figure. 12c) and mismatched degree ($p_1 = p_2 + 1$), respectively. For the
 734 distorted mesh, the proposed method with both global dual basis and Bézier
 735 dual basis perform similarly, the optimal convergence rates are reached for
 736 all cases. Some superconvergence behavior are observed (e.g. $p = 3$ for both
 737 global and Bézier dual basis). This partially due to the geometrical lock-
 738 ing existed in deformed meshes. For the mismatched mesh, the convergence
 739 performance of Bézier dual basis, though remains optimality, suffers a ver-
 740 tical lift of the error curves, which indicates that the Bézier dual basis are
 741 more sensitive to the mesh quality. However, for the finer mesh, the result
 742 obtained by 4^{th} order global dual basis become sub-optimal, we speculate
 743 this is caused by the $\inf - \sup$ instability in this specific circumstance. For
 744 the degree mismatched case, as expected, the convergence rates are between
 745 $p + 1$ and $p + 2$ in L^2 norm, and between $p - 1$ and p in H^2 norm for all
 746 tested cases.

747 Although a functional analysis of the contributions of the Lagrange mul-
 748 tipliers' best approximation error in the finite element approximation error is
 749 beyond the scope of this paper and postponed to future work, here we study
 750 their influence in a numerical manner. The best approximation of u in the
 751 discretized weak C^1 space \mathcal{K}_b^h can be given as: find $u \in \mathcal{K}_b^h$ such that

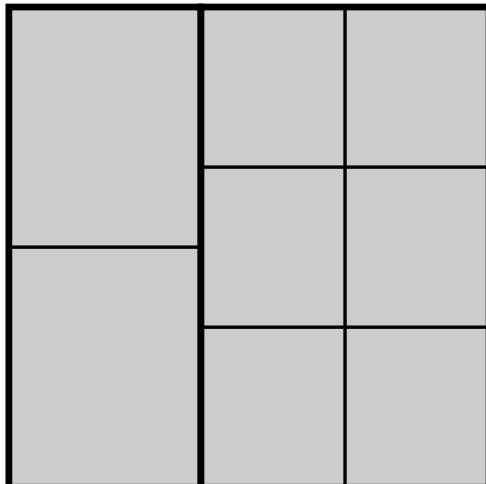
$$\langle v^h, u^h \rangle_{H^2} = \langle v^h, u \rangle_{H^2} \quad \forall v^h \in \mathcal{K}_b^h. \quad (80)$$

752 The best H^2 approximation error for the proposed methods for all sce-
753 narios are shown in Fig. 17. As can be seen, the convergence plots of the best
754 H^2 approximation error are identical to that of the finite element approxi-
755 mation error in H^2 norm. The best H^2 approximation errors for all cases are
756 no more than 1% smaller than that of the finite element counterparts, which
757 confirms our speculation that the contribution of the Lagrange multipliers'
758 best approximation errors are negligible for tested problems. In addition, the
759 best approximation error for the $p = 5$ global dual basis in the mismatched
760 non-conforming mesh test case also suffers rate decay, which confirms that
761 the main cause of the rate decay is due to the $\inf - \sup$ instability.

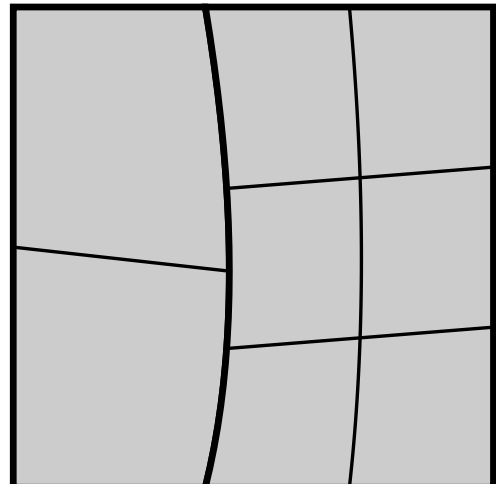
762 7.3. *Biharmonic problemon a three-patch domain with homogeneous Dirich-
763 let Boundary*

764 8. Schedule

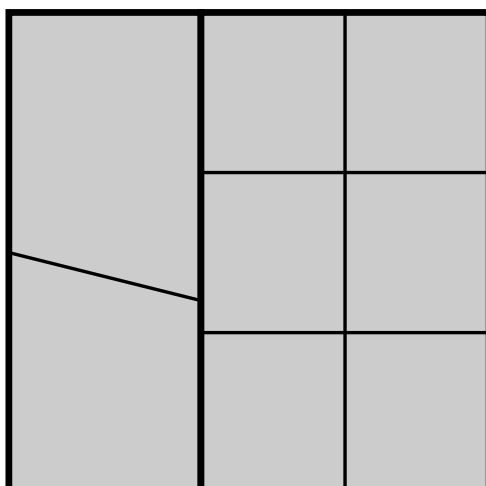
765 Although there are various aspects in weak C^1/G^1 coupling deserve a
766 thorough study, our main focus in this stage is to extend our finding in an ab-
767 abstract problem (biharmonic problem) to practical problems (e.g. Kirchhoff-
768 Love shell). Compared to the planar biharmonic problem, Kirchhoff-Love
769 shell is a more challenging problem, as the computational domain is in \mathbb{R}^3
770 and the constraint is not isotropically applied in each direction. Hence, a
771 more generalized constraint is needed to compromise geometries with kinks.
772 And validations are needed for two-patch and multi-patch Kirchhoff-Love
773 shells. Meanwhile, although we have implemented two algorithms to solve
774 multi-patch biharmonic problems, the boundary modification method does
775 not deliver ideal results while an additional factorization is needed for ex-
776 plicitly solving the null space. We will still make efforts in finding a feasi-
777 ble boundary modification for multi-patch coupling. A detailed time line is
778 shown in Table. 2.



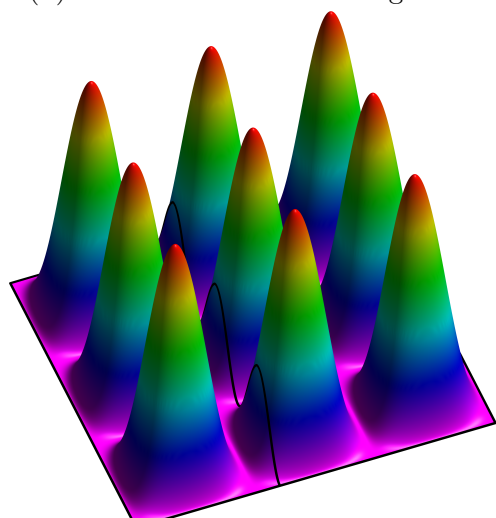
(a) Simple non-conforming mesh



(b) Distorted non-conforming mesh



(c) mismatched non-conforming mesh



(d) Reference solution

Figure 12: The discretizations of computational domain Ω and the manufactured solution with the property $u = \frac{\partial u}{\partial \mathbf{n}} = 0$ on $\partial\Omega$, which are used in Section 7.2.

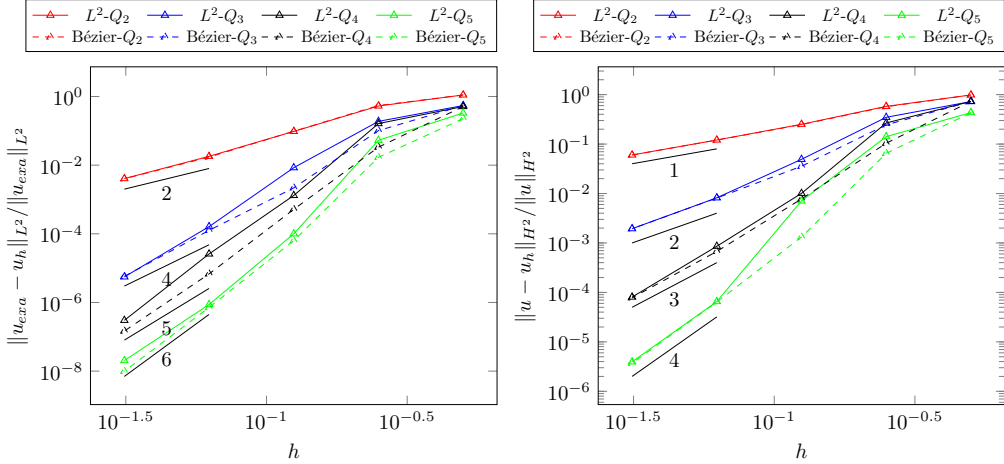


Figure 13: Convergence plot for simple non-conforming patch coupling in 7.2. Left: error measured in L^2 norm. Right: error measured in H^2 norm.

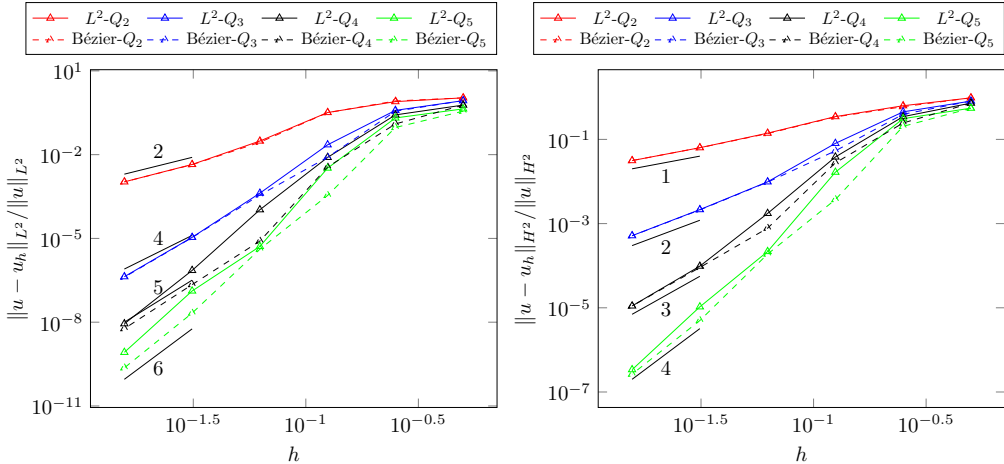


Figure 14: Convergence plot for distorted non-conforming patch coupling in 7.2. Left: error measured in L^2 norm. Right: error measured in H^2 norm.

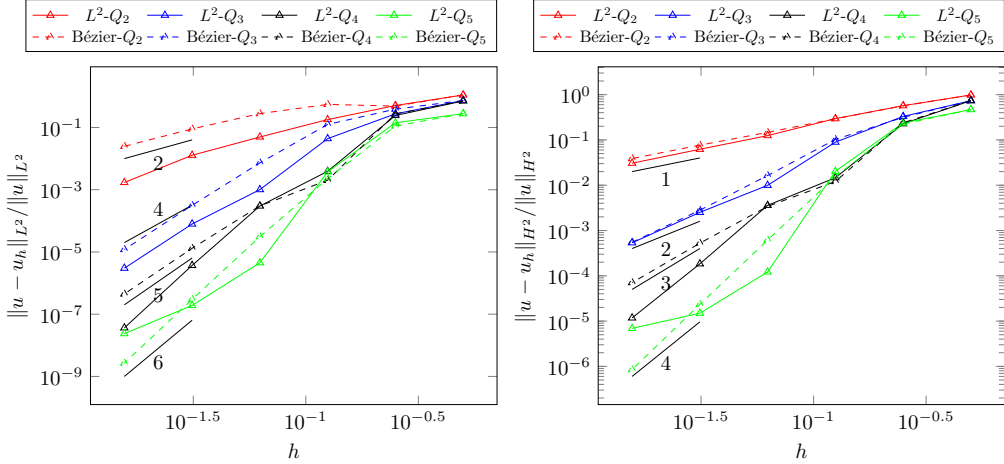


Figure 15: Convergence plot for mesh mismatched non-conforming patch coupling in 7.2. Left: error measured in L^2 norm. Right: error measured in H^2 norm.

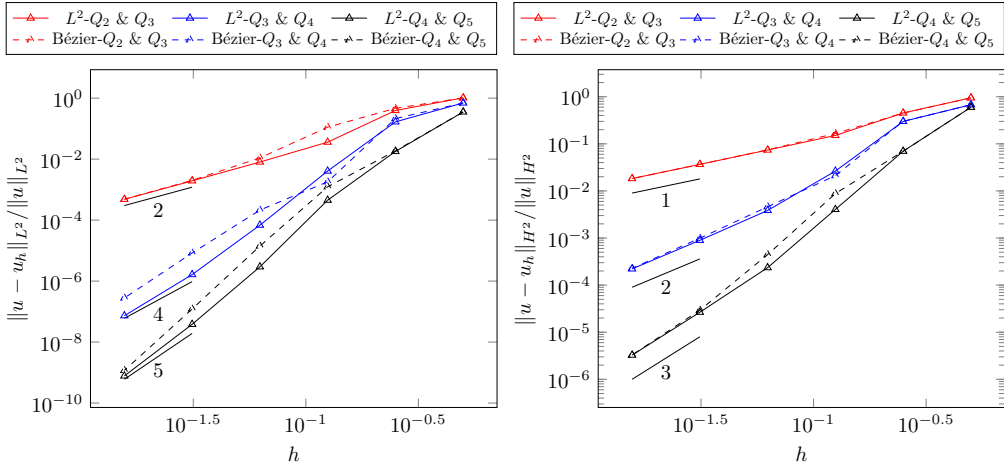


Figure 16: Convergence plot for degree mismatched non-conforming patch coupling in 7.2. Left: error measured in L^2 norm. Right: error measured in H^2 norm.

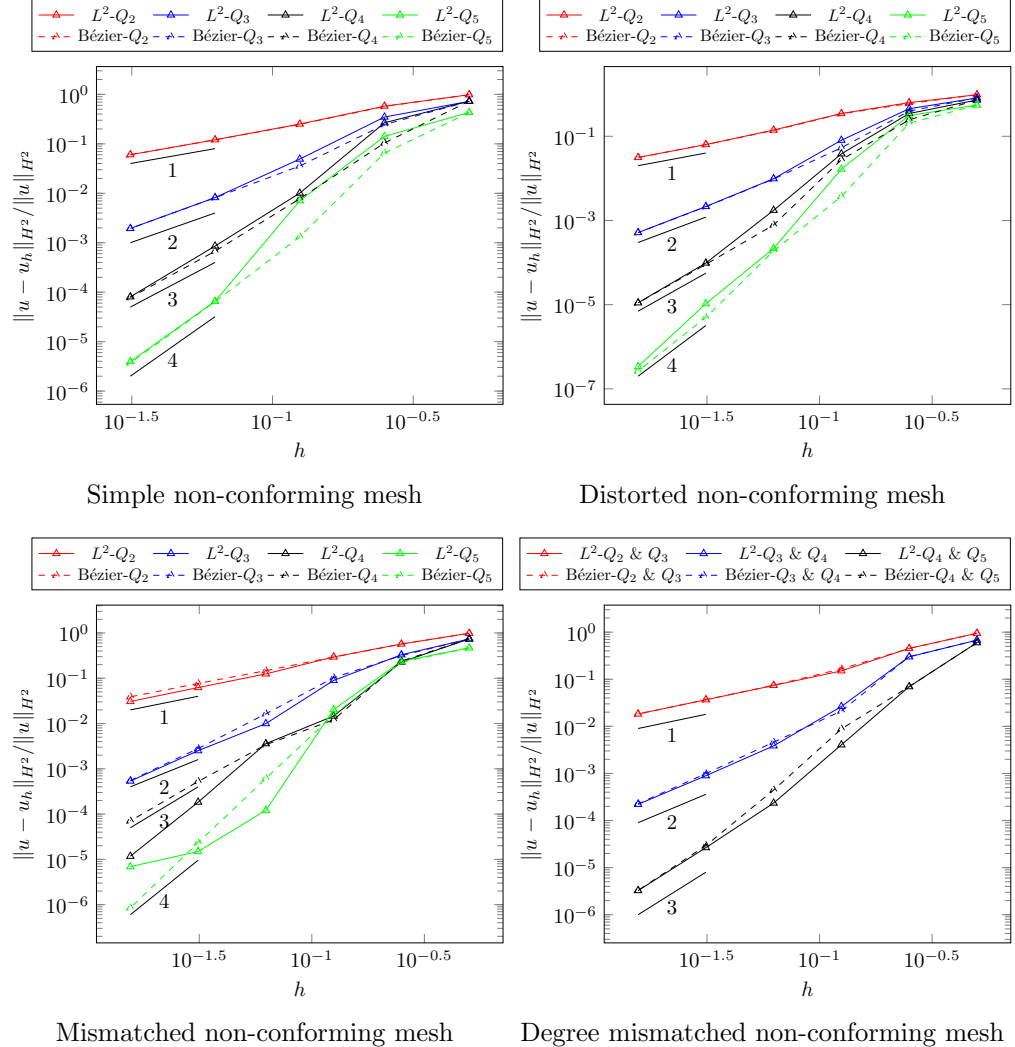
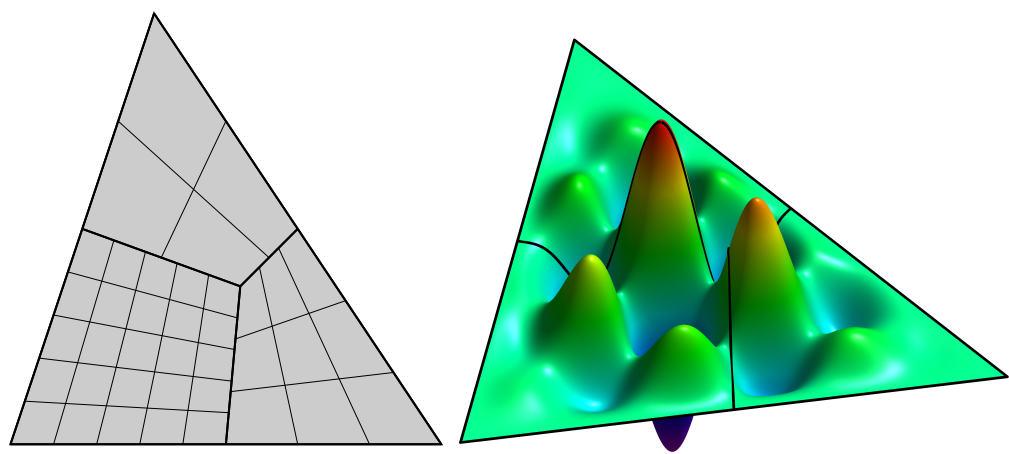


Figure 17: Convergence plot of the best H^2 approximation error for non-conforming patch coupling in 7.2.

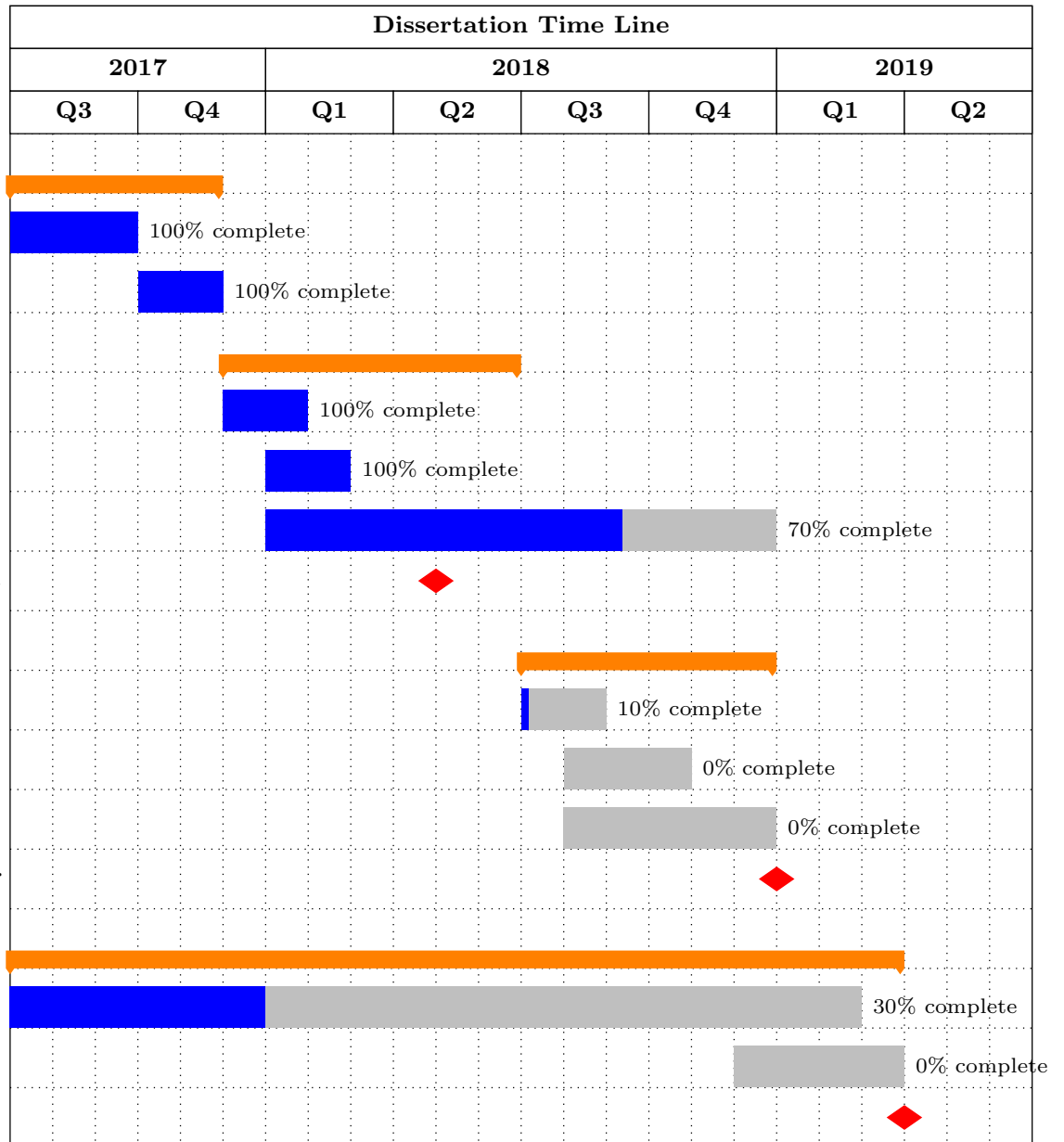


(a) Non-conforming mesh

(b) Reference solution

Figure 18: Convergence plot of the best H^2 approximation error for non-conforming patch coupling in 7.2.

Table 2: A schedule of tasks and stages of my research towards the final dissertation.



- 779 [1] Andreas Apostolatos, Michael Breitenberger, Roland Wüchner, and Kai-
 780 Uwe Bletzinger. Domain decomposition methods and kirchhoff-love shell
 781 multipatch coupling in isogeometric analysis. In *Isogeometric Analysis*
 782 and Applications 2014, pages 73–101. Springer, 2015.
- 783 [2] Andreas Apostolatos, Robert Schmidt, Roland Wüchner, and Kai-Uwe
 784 Bletzinger. A Nitsche-type formulation and comparison of the most
 785 common domain decomposition methods in isogeometric analysis. *International*
 786 *Journal for Numerical Methods in Engineering*, 97(7):473–504,
 787 February 2014.
- 788 [3] Helio JC Barbosa and Thomas JR Hughes. The finite element method
 789 with lagrange multipliers on the boundary: circumventing the babuška-
 790 brezzi condition. *Computer Methods in Applied Mechanics and Engi-*
 791 *neering*, 85(1):109–128, 1991.
- 792 [4] Y. Bazilevs, V. M. Calo, J. A. Cottrell, J. A. Evans, T. J. R. Hughes,
 793 S. Lipton, M. A. Scott, and T. W. Sederberg. Isogeometric analysis using
 794 T-splines. *Computer Methods in Applied Mechanics and Engineering*,
 795 199(5–8):229–263, January 2010.
- 796 [5] Yuri Bazilevs, L Beirao da Veiga, J Austin Cottrell, Thomas JR Hughes,
 797 and Giancarlo Sangalli. Isogeometric analysis: approximation, stabil-
 798 ity and error estimates for h-refined meshes. *Mathematical Models and*
 799 *Methods in Applied Sciences*, 16(07):1031–1090, 2006.
- 800 [6] Roland Becker, Peter Hansbo, and Rolf Stenberg. A finite ele-
 801 ment method for domain decomposition with non-matching grids.
 802 *ESAIM: Mathematical Modelling and Numerical Analysis - Modélisation*
 803 *Mathématique et Analyse Numérique*, 37(2):209–225, 2003.
- 804 [7] F. B. Belgacem, P. Hild, and P. Laborde. The mortar finite element
 805 method for contact problems. *Mathematical and Computer Modelling*,
 806 28(4):263–271, August 1998.
- 807 [8] Faker Ben Belgacem. The Mortar finite element method with Lagrange
 808 multipliers. *Numerische Mathematik*, 84(2):173–197, December 1999.
- 809 [9] FAKER BEN BELGACEM, Patrick Hild, and Patrick Laborde. Ex-
 810 tension of the mortar finite element method to a variational inequality

- 811 modeling unilateral contact. *Mathematical Models and Methods in Applied Sciences*, 9(02):287–303, 1999.
- 812
- 813 [10] Zakaria Belhachmi and Christine Bernardi. Resolution of fourth-order
814 problems by the mortar element method. *Computer Methods in Applied Mechanics and Engineering*, 116(1):53–58, January 1994.
- 815
- 816 [11] Michele Benzi and Andrew J. Wathen. Some Preconditioning Techniques for Saddle Point Problems. In Wilhelmus H. A. Schilders, Henk A. van der Vorst, and Joost Rommes, editors, *Model Order Reduction: Theory, Research Aspects and Applications*, number 13 in Mathematics in Industry, pages 195–211. Springer Berlin Heidelberg, 2008. DOI: 10.1007/978-3-540-78841-6_10.
- 817
- 818
- 819
- 820
- 821
- 822 [12] Michel Bercovier and Tanya Matskewich. Smooth Bezier Surfaces over Arbitrary Quadrilateral Meshes. *arXiv:1412.1125 [math]*, December 2014. arXiv: 1412.1125.
- 823
- 824
- 825 [13] C. Bernardi, Y. Maday, and A. T. Patera. Domain Decomposition by the Mortar Element Method. In Hans G. Kaper, Marc Garbey, and Gail W. Pieper, editors, *Asymptotic and Numerical Methods for Partial Differential Equations with Critical Parameters*, pages 269–286. Springer Netherlands, Dordrecht, 1993. DOI: 10.1007/978-94-011-1810-1_17.
- 826
- 827
- 828
- 829
- 830 [14] Christine Bernardi, Yvon Maday, and Francesca Rapetti. Basics and some applications of the mortar element method. *GAMM-Mitteilungen*, 28(2):97–123, November 2005.
- 831
- 832
- 833 [15] Daniele Boffi, Franco Brezzi, and Michel Fortin. *Mixed Finite Element Methods and Applications*. Springer Series in Computational Mathematics. Springer-Verlag.
- 834
- 835
- 836 [16] Michael J Borden, Thomas JR Hughes, Chad M Landis, and Clemens V Verhoosel. A higher-order phase-field model for brittle fracture: Formulation and analysis within the isogeometric analysis framework. *Computer Methods in Applied Mechanics and Engineering*, 273:100–118, 2014.
- 837
- 838
- 839
- 840
- 841 [17] Michael J Borden, Clemens V Verhoosel, Michael A Scott, Thomas JR Hughes, and Chad M Landis. A phase-field description of dynamic brit-
- 842

- 843 tle fracture. *Computer Methods in Applied Mechanics and Engineering*,
 844 217:77–95, 2012.
- 845 [18] P. B. Bornemann and F. Cirak. A subdivision-based implementation of
 846 the hierarchical b-spline finite element method. *Computer Methods in*
 847 *Applied Mechanics and Engineering*, 253:584–598, January 2013.
- 848 [19] Robin Bouclier, Jean-Charles Passieux, and Michel Salaün. Develop-
 849 ment of a new, more regular, mortar method for the coupling of NURBS
 850 subdomains within a NURBS patch: Application to a non-intrusive local
 851 enrichment of NURBS patches. *Computer Methods in Applied Mechan-*
 852 *ics and Engineering*, 316:123–150, April 2017.
- 853 [20] Susanne Brenner and Ridgway Scott. *The Mathematical Theory of Fi-*
 854 *nite Element Methods*. Springer Science & Business Media, December
 855 2007. Google-Books-ID: ci4c_R0WKYYC.
- 856 [21] Ericka Brivadis, Annalisa Buffa, Barbara Wohlmuth, and Linus Wun-
 857 derlich. Isogeometric mortar methods. *Computer Methods in Applied*
 858 *Mechanics and Engineering*, 284:292–319, February 2015.
- 859 [22] A. Buffa, D. Cho, and G. Sangalli. Linear independence of the T-spline
 860 blending functions associated with some particular T-meshes. *Computer*
 861 *Methods in Applied Mechanics and Engineering*, 199(23–24):1437–1445,
 862 April 2010.
- 863 [23] E. Catmull and J. Clark. Recursively generated B-spline surfaces on
 864 arbitrary topological meshes. *Computer-Aided Design*, 10(6):350–355,
 865 November 1978.
- 866 [24] Franz Chouly, Patrick Hild, and Yves Renard. Symmetric and non-
 867 symmetric variants of Nitsche’s method for contact problems in elasticity:
 868 theory and numerical experiments. *Mathematics of Computation*,
 869 84(293):1089–1112, 2015.
- 870 [25] Annabelle Collin, Giancarlo Sangalli, and Thomas Takacs. Analysis-
 871 suitable G1 multi-patch parametrizations for C1 isogeometric spaces.
 872 *Computer Aided Geometric Design*, 47:93–113, October 2016.
- 873 [26] Laurens Coox, Onur Atak, Dirk Vandepitte, and Wim Desmet. An isoge-
 874 ometric indirect boundary element method for solving acoustic problems

- 875 in open-boundary domains. *Computer Methods in Applied Mechanics*
 876 and *Engineering*, 316:186–208, April 2017.
- 877 [27] Laurens Coox, Francesco Greco, Onur Atak, Dirk Vandepitte, and Wim
 878 Desmet. A robust patch coupling method for NURBS-based isogeometric
 879 analysis of non-conforming multipatch surfaces. *Computer Methods*
 880 in *Applied Mechanics and Engineering*, 316:235–260, April 2017.
- 881 [28] Laurens Coox, Florian Maurin, Francesco Greco, Elke Deckers, Dirk
 882 Vandepitte, and Wim Desmet. A flexible approach for coupling nurbs
 883 patches in rotationless isogeometric analysis of kirchhoff–love shells.
 884 *Computer Methods in Applied Mechanics and Engineering*, 325:505–531,
 885 2017.
- 886 [29] L Beirao Da Veiga, Annalisa Buffa, Judith Rivas, and Giancarlo Sangalli.
 887 Some estimates for h–p–k-refinement in isogeometric analysis. *Nu-
 888 merische Mathematik*, 118(2):271–305, 2011.
- 889 [30] L Beirao Da Veiga, Annalisa Buffa, Giancarlo Sangalli, and Rafael
 890 Vázquez. Mathematical analysis of variational isogeometric methods.
 891 *Acta Numerica*, 23:157–287, 2014.
- 892 [31] D. Doo and M. Sabin. Behaviour of recursive division surfaces near ex-
 893 traordinary points. *Computer-Aided Design*, 10(6):356–360, November
 894 1978.
- 895 [32] W Dornisch, J Stöckler, and R Müller. Dual and approximate dual
 896 basis functions for b-splines and nurbs—comparison and application for
 897 an efficient coupling of patches with the isogeometric mortar method.
 898 *Computer Methods in Applied Mechanics and Engineering*, 316:449–496,
 899 2017.
- 900 [33] W. Dornisch, J. Stöckler, and R. Müller. Dual and approximate dual
 901 basis functions for B-splines and NURBS – Comparison and application
 902 for an efficient coupling of patches with the isogeometric mortar method.
 903 *Computer Methods in Applied Mechanics and Engineering*, 316:449–496,
 904 April 2017.
- 905 [34] W. Dornisch, G. Vitucci, and S. Klinkel. The weak substitution method
 906 – an application of the mortar method for patch coupling in NURBS–

- 907 based isogeometric analysis. *International Journal for Numerical Methods in Engineering*, 103(3):205–234, July 2015.
- 908
- 909 [35] Wolfgang Dornisch and Sven Klinkel. Boundary conditions and multi-
910 patch connections in isogeometric analysis. *PAMM*, 11(1):207–208, 2011.
- 911 [36] Wolfgang Dornisch and Ralf Müller. Patch coupling with the isogeomet-
912 ric dual mortar approach. *PAMM*, 16(1):193–194, October 2016.
- 913 [37] Michael R. Dörfel, Bert Jüttler, and Bernd Simeon. Adaptive isogeomet-
914 ric analysis by local h-refinement with T-splines. *Computer Methods in
915 Applied Mechanics and Engineering*, 199(5–8):264–275, January 2010.
- 916 [38] Anand Embar, John Dolbow, and Isaac Harari. Imposing Dirichlet
917 boundary conditions with Nitsche’s method and spline-based finite el-
918 ements. *International Journal for Numerical Methods in Engineering*,
919 83(7):877–898, August 2010.
- 920 [39] Charbel Farhat, Po-Shu Chen, and Jan Mandel. A scalable Lagrange
921 multiplier based domain decomposition method for time-dependent
922 problems. *International Journal for Numerical Methods in Engineering*,
923 38(22):3831–3853, November 1995.
- 924 [40] David R. Forsey and Richard H. Bartels. Hierarchical B-spline Re-
925 finement. In *Proceedings of the 15th Annual Conference on Computer
926 Graphics and Interactive Techniques*, SIGGRAPH ’88, pages 205–212,
927 New York, NY, USA, 1988. ACM.
- 928 [41] Carlotta Giannelli, Bert Jüttler, and Hendrik Speleers. THB-splines:
929 The truncated basis for hierarchical splines. *Computer Aided Geometric
930 Design*, 29(7):485–498, October 2012.
- 931 [42] Héctor Gómez, Victor M Calo, Yuri Bazilevs, and Thomas JR Hughes.
932 Isogeometric analysis of the cahn–hilliard phase-field model. *Computer
933 methods in applied mechanics and engineering*, 197(49–50):4333–4352,
934 2008.
- 935 [43] David Groisser and Jörg Peters. Matched -constructions always yield
936 -continuous isogeometric elements. *Computer Aided Geometric Design*,
937 34:67–72, March 2015.

- 938 [44] Yujie Guo and Martin Ruess. Nitsche's method for a coupling of isogeometric thin shells and blended shell structures. *Computer Methods in*
 939 *Applied Mechanics and Engineering*, 284:881–905, February 2015.
- 941 [45] Peter Hansbo. Nitsche's method for interface problems in computational mechanics. *GAMM-Mitteilungen*, 28(2):183–206, November 2005.
 942
- 943 [46] Peter Hansbo, Carlo Lovadina, Ilaria Perugia, and Giancarlo Sangalli. A
 944 lagrange multiplier method for the finite element solution of elliptic interface problems using non-matching meshes. *Numerische Mathematik*,
 945 100(1):91–115, 2005.
 946
- 947 [47] Christian Hesch and Peter Betsch. Isogeometric analysis and domain
 948 decomposition methods. *Computer Methods in Applied Mechanics and*
 949 *Engineering*, 213–216:104–112, March 2012.
- 950 [48] Stefan Hüeber and Barbara I Wohlmuth. A primal–dual active set strategy
 951 for non-linear multibody contact problems. *Computer Methods in*
 952 *Applied Mechanics and Engineering*, 194(27–29):3147–3166, 2005.
- 953 [49] T.J.R. Hughes, J.A. Cottrell, and Y. Bazilevs. Isogeometric analysis:
 954 Cad, finite elements, nurbs, exact geometry and mesh refinement. *Computer*
 955 *Methods in Applied Mechanics and Engineering*, 194(39):4135 –
 956 4195, 2005.
- 957 [50] Mika Juntunen. On the connection between the stabilized lagrange multipler and nitsche's methods. *Numerische Mathematik*, 131(3):453–471,
 958 2015.
 959
- 960 [51] Bert Jüttler, Angelos Mantzaflaris, Ricardo Perl, and Martin Rumpf.
 961 On numerical integration in isogeometric subdivision methods for PDEs
 962 on surfaces. *Computer Methods in Applied Mechanics and Engineering*,
 963 302:131–146, April 2016.
- 964 [52] Hongmei Kang, Xin Li, Falai Chen, and Jiansong Deng. Truncated
 965 Hierarchical Loop Subdivision Surfaces and application in isogeometric
 966 analysis. *Computers & Mathematics with Applications*, 72(8):2041–2055,
 967 October 2016.
- 968 [53] Mario Kapl, Florian Buchegger, Michel Bercovier, and Bert Jüttler. Iso-
 969 geometric analysis with geometrically continuous functions on planar

- 970 multi-patch geometries. *Computer Methods in Applied Mechanics and*
 971 *Engineering*, 316:209–234, April 2017.
- 972 [54] Mario Kapl and Vito Vitrih. Space of -smooth geometrically continuous
 973 isogeometric functions on planar multi-patch geometries: Dimension and
 974 numerical experiments. *Computers & Mathematics with Applications*.
- 975 [55] Mario Kapl and Vito Vitrih. Space of -smooth geometrically continuous
 976 isogeometric functions on two-patch geometries. *Computers & Mathe-*
 977 *matics with Applications*, 73(1):37–59, January 2017.
- 978 [56] Mario Kapl, Vito Vitrih, Bert Jüttler, and Katharina Birner. Isoge-
 979 ometric analysis with geometrically continuous functions on two-patch
 980 geometries. *Computers & Mathematics with Applications*, 70(7):1518–
 981 1538, October 2015.
- 982 [57] J Kiendl, Y Bazilevs, M-C Hsu, R Wüchner, and K-U Bletzinger. The
 983 bending strip method for isogeometric analysis of kirchhoff–love shell
 984 structures comprised of multiple patches. *Computer Methods in Applied*
 985 *Mechanics and Engineering*, 199(37-40):2403–2416, 2010.
- 986 [58] J Kiendl, K-U Bletzinger, J Linhard, and R Wüchner. Isogeometric shell
 987 analysis with kirchhoff–love elements. *Computer Methods in Applied*
 988 *Mechanics and Engineering*, 198(49-52):3902–3914, 2009.
- 989 [59] Josef Kiendl, Ming-Chen Hsu, Michael CH Wu, and Alessandro Reali.
 990 Isogeometric kirchhoff–love shell formulations for general hyperelastic
 991 materials. *Computer Methods in Applied Mechanics and Engineering*,
 992 291:280–303, 2015.
- 993 [60] Bishnu Prasad Lamichhane. Higher order mortar finite elements with
 994 dual lagrange multiplier spaces and applications.
- 995 [61] Bishnu Prasad Lamichhane and Barbara I Wohlmuth. Higher order
 996 dual lagrange multiplier spaces for mortar finite element discretizations.
Calcolo, 39(4):219–237, 2002.
- 998 [62] Xin Li and M. A. Scott. Analysis-suitable T-splines: Characterization,
 999 refineability, and approximation. *Mathematical Models and Methods in*
 1000 *Applied Sciences*, 24(06):1141–1164, October 2013.

- 1001 [63] Xin Li, Jianmin Zheng, Thomas W. Sederberg, Thomas J. R. Hughes,
 1002 and Michael A. Scott. On linear independence of T-spline blending func-
 1003 tions. *Computer Aided Geometric Design*, 29(1):63–76, January 2012.
- 1004 [64] Charles Teorell Loop and Charles Loop. Smooth Subdivision Surfaces
 1005 Based on Triangles. January 1987.
- 1006 [65] Leszek Marcinkowski. Mortar methods for some second and fourth order
 1007 elliptic equations. *Distinguished Ph. D. Thesis*, 1999.
- 1008 [66] Stephen E Moore. Discontinuous galerkin isogeometric analysis for the
 1009 biharmonic equation. *arXiv preprint arXiv:1703.02726*, 2017.
- 1010 [67] Thien Nguyen, Keçstutis Karčiauskas, and Jörg Peters. A Comparative
 1011 Study of Several Classical, Discrete Differential and Isogeometric Meth-
 1012 ods for Solving Poisson’s Equation on the Disk. *Axioms*, 3(2):280–299,
 1013 June 2014.
- 1014 [68] Vinh Phu Nguyen, Pierre Kerfriden, Marco Brino, Stéphane P. A. Bor-
 1015 das, and Elvio Bonisoli. Nitsche’s method for two and three dimensional
 1016 NURBS patch coupling. *Computational Mechanics*, 53(6):1163–1182,
 1017 June 2014.
- 1018 [69] J. Nitsche. Über ein Variationsprinzip zur Lösung von Dirichlet-
 1019 Problemen bei Verwendung von Teilräumen, die keinen Randbedingun-
 1020 gen unterworfen sind. *Abhandlungen aus dem Mathematischen Seminar
 1021 der Universität Hamburg*, 36(1):9–15, July 1971.
- 1022 [70] Peter Oswald and Barbara Wohlmuth. On polynomial reproduction of
 1023 dual fe bases. In *Thirteenth international conference on domain decom-
 1024 position methods*, pages 85–96, 2001.
- 1025 [71] Qing Pan, Guoliang Xu, Gang Xu, and Yongjie Zhang. Isogeometric
 1026 analysis based on extended Loop’s subdivision. *Journal of Compu-
 1027 tational Physics*, 299:731–746, October 2015.
- 1028 [72] Jörg Peters. Joining smooth patches around a vertex to form a C_k
 1029 surface. *Computer Aided Geometric Design*, 9(5):387–411, November
 1030 1992.

- 1031 [73] Jörg Peters. Chapter 8 - Geometric Continuity. In *Handbook of Computer Aided Geometric Design*, pages 193–227. North-Holland, Amsterdam, 2002. DOI: 10.1016/B978-044451104-1/50009-5.
- 1032
1033
- 1034 [74] Alexander Popp, Michael W Gee, and Wolfgang A Wall. A finite de-
1035 formation mortar contact formulation using a primal–dual active set
1036 strategy. *International Journal for Numerical Methods in Engineering*,
1037 79(11):1354–1391, 2009.
- 1038
1039
- 1040 [75] Beatrice Riviere. *Discontinuous Galerkin methods for solving elliptic*
1041 *and parabolic equations: theory and implementation*. SIAM, 2008.
- 1042
1043
- 1044 [76] M. A. Scott, X. Li, T. W. Sederberg, and T. J. R. Hughes. Local
1045 refinement of analysis-suitable T-splines. *Computer Methods in Applied*
1046 *Mechanics and Engineering*, 213–216:206–222, March 2012.
- 1047
1048
- 1049 [77] M. A. Scott, R. N. Simpson, J. A. Evans, S. Lipton, S. P. A. Bordas,
1050 T. J. R. Hughes, and T. W. Sederberg. Isogeometric boundary element
1051 analysis using unstructured T-splines. *Computer Methods in Applied*
1052 *Mechanics and Engineering*, 254:197–221, February 2013.
- 1053
1054
- 1055 [78] Michael A. Scott, Michael J. Borden, Clemens V. Verhoosel, Thomas W.
1056 Sederberg, and Thomas J. R. Hughes. Isogeometric finite element data
1057 structures based on Bézier extraction of T-splines. *International Journal*
1058 *for Numerical Methods in Engineering*, 88(2):126–156, October 2011.
- 1059
1060
- 1061 [79] Thomas W. Sederberg, Jianmin Zheng, Almaz Bakenov, and Ahmad
1062 Nasri. T-splines and T-NURCCs. In *ACM SIGGRAPH 2003 Papers*,
1063 SIGGRAPH ’03, pages 477–484, New York, NY, USA, 2003. ACM.
- 1064
1065
- 1066 [80] Alexander Seitz, Philipp Farah, Johannes Kremheller, Barbara I.
1067 Wohlmuth, Wolfgang A. Wall, and Alexander Popp. Isogeometric dual
1068 mortar methods for computational contact mechanics. *Computer Meth-
1069 odks in Applied Mechanics and Engineering*, 301:259–280, April 2016.
- 1070
1071
- 1072 [81] Juan C Simo, Peter Wriggers, and Robert L Taylor. A perturbed la-
1073 grangian formulation for the finite element solution of contact problems.
1074 *Computer methods in applied mechanics and engineering*, 50(2):163–180,
1075 1985.
- 1076
1077

- 1062 [82] Rolf Stenberg. On some techniques for approximating boundary con-
 1063 ditions in the finite element method. *Journal of Computational and*
 1064 *applied Mathematics*, 63(1-3):139–148, 1995.
- 1065 [83] Gilbert Strang and George Fix. *An Analysis of the Finite Element*
 1066 *Method*. Wellesley-Cambridge Press, May 2008. Google-Books-ID:
 1067 K5MAOwAACAAJ.
- 1068 [84] Radek Tezaur. *Analysis of Lagrange multiplier based domain decompo-*
 1069 *sition*. PhD thesis, University of Colorado at Denver, 1998.
- 1070 [85] Derek C Thomas, Michael A Scott, John A Evans, Kevin Tew, and
 1071 Emily J Evans. Bézier projection: a unified approach for local pro-
 1072 jection and quadrature-free refinement and coarsening of nurbs and t-
 1073 splines with particular application to isogeometric design and analysis.
 1074 *Computer Methods in Applied Mechanics and Engineering*, 284:55–105,
 1075 2015.
- 1076 [86] Manuel Tur, Jose Albelda, Jose Manuel Navarro-Jimenez, and Juan Jose
 1077 Rodenas. A modified perturbed lagrangian formulation for contact prob-
 1078 lems. *Computational Mechanics*, 55(4):737–754, 2015.
- 1079 [87] A. V. Vuong, C. Giannelli, B. Jüttler, and B. Simeon. A hierarchical ap-
 1080 proach to adaptive local refinement in isogeometric analysis. *Computer*
 1081 *Methods in Applied Mechanics and Engineering*, 200(49–52):3554–3567,
 1082 December 2011.
- 1083 [88] Xiaodong Wei, Yongjie Zhang, Thomas J. R. Hughes, and Michael A.
 1084 Scott. Truncated hierarchical Catmull–Clark subdivision with local re-
 1085 finement. *Computer Methods in Applied Mechanics and Engineering*,
 1086 291:1–20, July 2015.
- 1087 [89] B. Wohlmuth. A Mortar Finite Element Method Using Dual Spaces
 1088 for the Lagrange Multiplier. *SIAM Journal on Numerical Analysis*,
 1089 38(3):989–1012, January 2000.
- 1090 [90] Barbara I Wohlmuth. A comparison of dual lagrange multiplier spaces
 1091 for mortar finite element discretizations. *ESAIM: Mathematical Mod-
 1092 ell ing and Numerical Analysis*, 36(6):995–1012, 2002.

- 1093 [91] Xin Li. Some Properties for Analysis-Suitable T-Splines. *Journal of*
1094 *Computational Mathematics*, 33(4):428–442, July 2015.
- 1095 [92] Olgierd Cecil Zienkiewicz, Robert Leroy Taylor, Olgierd Cecil
1096 Zienkiewicz, and Robert Lee Taylor. *The finite element method*, vol-
1097 ume 3. McGraw-hill London, 1977.